Article

Development of Potent and Selective Antagonists for the UTP-Activated P2Y Receptor

Muhammad Rafehi, Enas Malik, Alexander Neumann, Aliaa Abdelrahman,
Theodor Hanck, Vigneshwaran Namasivayam, Christa E Müller, and Younis Baqi

Just Accepted

Development of Potent and Selective Antagonists for

the UTP-Activated P2Y$_4$ Receptor

Muhammad Rafehi,[†,#] Enas M. Malik, [†,#] Alexander Neumann,[†] Aliaa Abdelrahman,[†] Theodor Hanck,[†] Vigneshwaran Namasivayam, [†] Christa E. Müller,[†] and Younis Baqi*[‡]*

[†]PharmaCenter Bonn, Pharmaceutical Institute, Pharmaceutical Chemistry I, Pharmaceutical

Sciences Bonn (PSB), University of Bonn, An der Immenburg 4, D-53121 Bonn, [‡]Department

of Chemistry, Faculty of Science, Sultan Qaboos University, PO Box 36, Postal Code 123,

Muscat, Oman

[#]These authors contributed equally to this work

ABSTRACT. P2Y$_4$ is a G$_q$ protein-coupled receptor activated by uridine-5'-triphosphate (UTP), which is widely expressed in the body, e.g., in intestine, heart, and brain. No selective P2Y$_4$ receptor antagonist has been described so far. Therefore, we developed and optimized P2Y$_4$ antagonists based on an anthraquinone scaffold. Potency was assessed by a fluorescence-based assay measuring inhibition of UTP-induced intracellular calcium release in 1321N1 astrocytoma cells stably transfected with the human P2Y$_4$ receptor. The most potent compound of the present series, sodium 1-amino-4-[4-(2,4-dimethylphenylthio)phenylamino]-9,10-dioxo-9,10-dihydroanthracene-2-sulfonate (PSB-16133, **61**) exhibited an IC$_{50}$ value of 233 nM, selectivity versus other P2Y receptor subtypes, and is thought to act as an allosteric antagonist. A receptor homology model was built and docking studies were performed to analyze ligand-receptor interactions. Compound **64** represents the most potent and selective P2Y$_4$ receptor antagonist known to date and is therefore anticipated to become a useful tool for studying this scarcely investigated receptor.

KEYWORDS. anthraquinone, cystic fibrosis, infectious diarrhea, homology modeling, neurodegenerative diseases, P2Y$_4$ antagonist, Reactive Blue 2, selectivity, synthesis

Introduction

The G protein-coupled P2Y receptors represent, together with the ATP-gated ion channels known as P2X receptors, the nucleotide-activated P2 receptor family. Eight subtypes of P2Y receptors are known to exist: $P2Y_1$, $P2Y_2$, $P2Y_4$, $P2Y_6$, and $P2Y_{11}$ belonging to the $P2Y_1$-like subgroup, and $P2Y_{12}$, $P2Y_{13}$, and $P2Y_{14}$ that are members of the $P2Y_{12}$-like subgroup of P2Y receptors.[1,2]

P2Y receptors are present in almost all human tissues, where they exert various biological functions. They are of great interest as (potential) therapeutic targets for several indications, including neurodegenerative disorders, pain, cancer, and cardiovascular diseases.[3,4] In fact, several antithrombotic drugs on the market, namely clopidogrel, prasugrel and ticagrelor, achieve their effect through inhibiting the human platelet $P2Y_{12}$ receptor.[5–7] Despite a generally strong interest in the P2Y receptor family, relatively little is known regarding the $P2Y_4$ subtype. This uridine-5'-triphosphate (UTP)–activated receptor shows a wide distribution in the body, including heart, gastrointestinal tract (GIT), central nervous system (CNS), skin, and ear (cochlea).[8–12] In the GIT, $P2Y_4$ receptors were demonstrated to mediate chloride (Cl^-) secretion in the jejunal epithelium, and therefore represent possible targets for the treatment of cystic fibrosis ($P2Y_4$ receptor agonists) and diarrhea ($P2Y_4$ receptor antagonists).[13–16] $P2Y_4$ receptors also appear to be involved in the regulation of amyloid precursor protein (APP) production and its release in the brain.[17] Since APP accumulation is associated with the progression of Alzheimer's disease, $P2Y_4$ receptor antagonists might be useful as therapeutic agents for this debilitating and yet incurable disorder.[17] In the heart, $P2Y_4$ receptors are expressed on cardiac endothelial cells; they were found to be important for cardiac endothelial cell growth and migration, as well as secretion of platelet-derived growth factor B (PDGF-B). Moreover, $P2Y_4$ receptor-knockout mice showed defective post-natal

cardiac development, including reduced heart weight. It has thus been postulated that $P2Y_4$

receptors could be possible targets to modulate angiogenesis, and regulate cardiac remodeling

and post-ischemic revascularization.[18] In the cochlea, $P2Y_4$ receptors are expressed in the

epithelial cells of Reissner's membrane, where they regulate Na^+ absorption upon noise

exposure,[8] and in the apical membrane, where they are involved in K^+ secretion across strial

marginal cell epithelium during stimulation of the cochlea by sound.[9]

So far, no selective antagonists for the $P2Y_4$ receptors have been described.[1] However, such a

compound is required as a pharmacological tool for receptor characterization and for studies

aimed at target validation.[19] Mouse and rat $P2Y_4$ receptors, which share 51 % and 83 %

sequence identity with the human $P2Y_4$ receptor,[12,20] are non-competitively antagonized by

PPADS (pyridoxalphosphate-6-azophenyl-2',4'-disulfonic acid, **1**, Figure 1), and also blocked

by Reactive Blue 2 (RB-2, **2**, Figure 1).[21,22] Rat $P2Y_4$ receptors, expressed in *Xenopus* oocytes,

were found to be weakly antagonized by suramin (**3**, Figure 1).[23] On the other hand, human

$P2Y_4$ receptors expressed in 1321N1 cells were ineffectively inhibited by PPADS and were

insensitive to suramin,[23] but were inhibited by RB-2 at micromolar concentrations.[24]

RB-2 is a well-known non-selective P2 receptor antagonist that has served as an important

pharmacological tool in the field of purinergic signaling.[25,26] Our laboratory has been

extensively working on the development of anthraquinone derivatives structurally related to

RB-2 as potent and selective antagonists of purine receptors and ectonucleotidases.[24,27–36] For

example, we have previously developed PSB-0739 (**4**, Figure 1),[30] an extremely potent and

selective, competitive $P2Y_{12}$ receptor antagonist (pA_2 of 9.8),[37] and PSB-1011 (**5**, Figure 1), a

competitive inhibitor of the rat P2X2 receptor with a K_i value of 79 nM.[31]
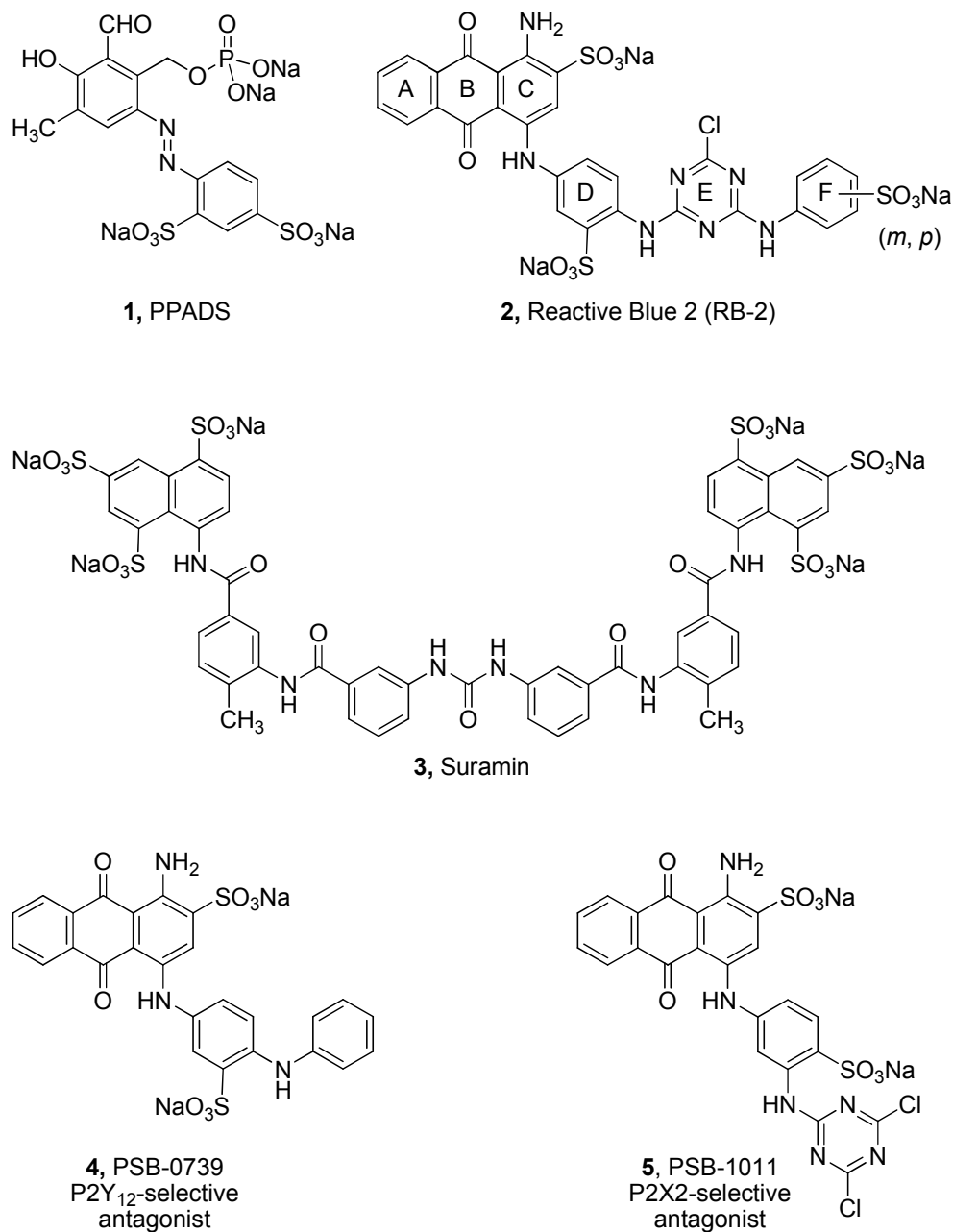
Figure 1. Structures of the classical P2 receptor antagonists PPADS, Reactive Blue 2 (RB-2), suramin, and receptor subtype-selective tool compounds derived from RB-2.

High potency and selectivity could be attained, for example, by optimizing the residue at the 4-position of the anthraquinone core. Structure-activity relationships (SARs) were found to be

very different at the different purine receptor subtypes, and the anthraquinone core structure can thus be described as a 'privileged structure' in medicinal chemistry.[26]

The aim of this study was to specifically design and develop the first potent and selective P2Y$_4$ receptor antagonist. To this end, a library of RB-2-related anthraquinone derivatives was synthesized using recently developed methods,[12–15] and the compounds were tested for their potency to block P2Y$_4$ receptors using a Ca^{2+}-mobilization assay.[16] This data served as a basis for subsequent structure-activity relationship analyses and receptor docking studies aimed at enhancing our knowledge with respect to P2Y$_4$ receptor ligand preferences and for further optimizing the structures. Modifications of the substituents at the 4-position of the anthraquinone core led to an increase in potency at the P2Y$_4$ receptor and resulted in selectivity for P2Y$_4$ over other P2Y receptor subtypes.

Results and discussion

Chemistry. The target compounds were synthesized as depicted in Schemes 1–3. The syntheses of several compounds had been previously described.[24,27–30,33,36,38–40] Some of the known anthraquinone derivatives (**19–21**, **24**, and **33–35** (Table 1)) have now been obtained by improved synthetic procedures. In addition to known compounds, a series of 21 new compounds was prepared. Condensation of bromaminic acid (R^1 = SO$_3$H (**6a**)) or 1-amino-4-bromo-2-methylanthraquinone (R^1 = CH$_3$ (**6b**)) with the appropriate amine yielded the target compounds in good to excellent isolated yields (Scheme 1). Reactions were conducted in phosphate buffer (pH 6-7) in the presence of copper powder (Cu^0) under microwave irradiation at 80-120 °C (in case of **6a** as a starting compound) or in methanol in the presence of potassium acetate and a mixture of Cu^0 and copper(II) acetate monohydrate under microwave irradiation at 95 °C (in case of **6b**).

1
2
3
4
5
6
7
8
9
10
11
12
13
14
15
16
17
18
19
20
21
22
23
24
25
26
27
28
29
30
31
32
33
34
35
36
37
38
39
40
41
42
43
44
45
46
47
48
49
50
51
52
53
54
55
56
57
58
59
60

Scheme 1. General Synthesis of 4-Substituted Anthraquinone Derivatives (**7–53** and **67**)[a]

6a, R^1 = SO$_3$Na
6b, R^1 = CH$_3$

7-53, 67
For **R^1, R^2** see Table 1
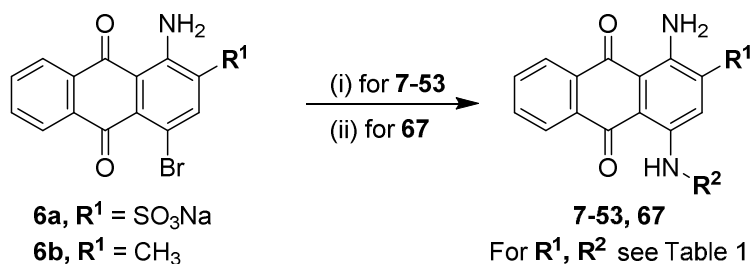
[a]Reagents and conditions: (i) R^2-NH$_2$, phosphate buffer (pH 6–7), Cu^0, microwave, 80-120 °C, 5-24 min; (ii) 2-amino-4-fluorobenzoic acid, methanol, potassium acetate, Cu^0, Cu(II) acetate, microwave, 95 °C, 70 min.

Compounds **65** and **66** were synthesized from 1-amino-4-bromo-2-methylanthraquinone (**6b**) by treatment with an excess of the appropriate aniline derivative (15 equiv.) under argon in the presence of potassium acetate and a catalytic amount of copper(I) acetate at 110 °C for 6-15 h (Scheme 2).

Scheme 2. Synthesis of Anthraquinone Derivatives **65** and **66**[a]

6b

65, R = 3-F
66, R = 3-OMe
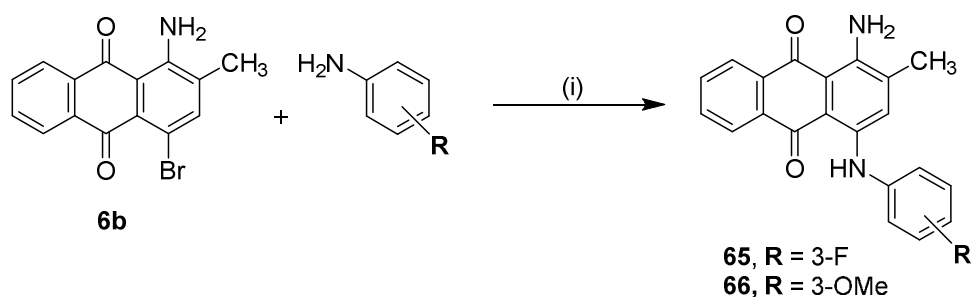
[a]Reagents and conditions: (i) CuOAc, KOAc, 110 °C, argon, 6–15 h.

Three anilinoanthraquinone derivatives, **12**, **27**, and **46**, which bear a primary amino group in the 1-position of the anthraquinone moiety, were treated with sodium nitrite in hydrochloric acid solution (1 M) at 0 °C for 5 min, then allowed to warm up to room temperature followed
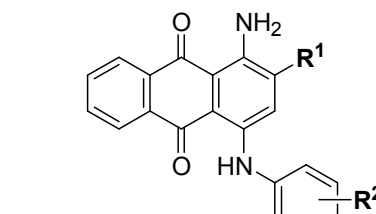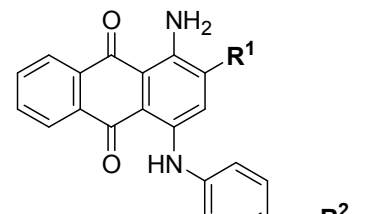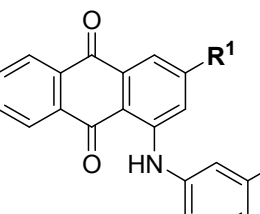
by the addition of ethanol and an excess of zinc powder (10 equiv.) to achieve deamination[39]

affording the desired products **68–70** (Scheme 3).

Scheme 3. Synthesis of Deaminated Anthraquinone Derivatives **68–70**[a]

13 R^1= R^3 = H, R^2 = F
27 R^1= R^3 = H, R^2 = OMe
46 R^1 = CO$_2$H, R^2 = H, R^3 = F

68 R^1= R^3 = H, R^2 = F
69 R^1= R^3 = H, R^2 = OMe
70 R^1 = CO$_2$H, R^2 = H, R^3 = F
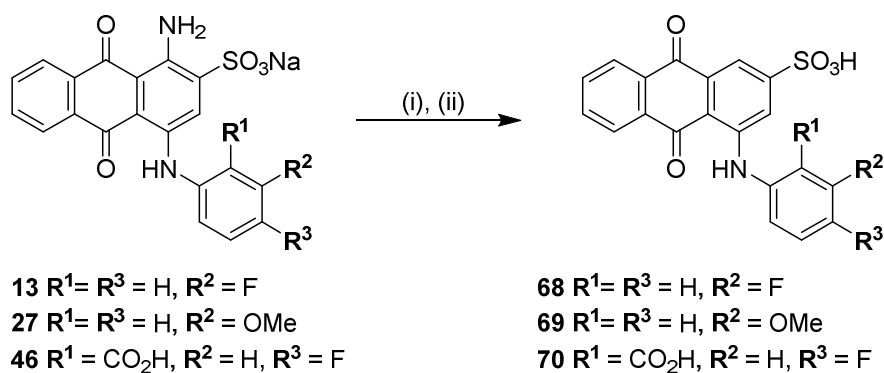
[a]Reagents and conditions: (i) NaNO$_2$, HCl (1 M), 0–5 °C, 5 min, (ii) Zn (10 equiv.), ethanol, rt, 30 s.

Table 1. Yields, Molecular Weights, UV Absorption, Color, and Purity of the Newly Synthesized Anthraquinone Derivatives

| | Structure A | Structure B | Structure C |

Compd	R^1	R^2 (A, C) or R^2-X (B)	Yield (%)[a]	MW (g/mol)	Absorption λ_{max} (nm)	Color	Purity by LC-MS/UV (%)[b]
	Structure A						
14	SO_3Na	2-chloro	36	450.83	590	Blue	99.0
19	SO_3Na	2-methyl	80	430.41	624	Blue	99.0
20	SO_3Na	3-methyl	70	430.41	626	Blue	99.1
21	SO_3Na	4-methyl	72	430.41	626	Blue	100.0
24	SO_3Na	4-ethyl	64	444.44	626	Blue	99.0
25	SO_3Na	3-propyl	35	458.46	628	Blue	97.7
33	SO_3Na	2,3-dimethyl	49	444.44	624	Blue	99.0
34	SO_3Na	2,4-dimethyl	60	444.44	624	Blue	99.0
35	SO_3Na	2,5-dimethyl	50	444.44	624	Blue	99.5
37	SO_3Na	3,4-dimethoxy	46	476.43	624	Blue	98.5

39	SO$_3$Na	3-methoxy-4-methyl	44	460.43	626	Blue	98.3
40	SO$_3$Na	4-chloro-2-methyl	36	464.85	626	Blue	99.0
41	SO$_3$Na	4-chloro-3-methyl	40	464.85	624	Blue	99.0
42	SO$_3$Na	4-hydroxy-3-methyl	40	446.41	626	Blue	96.0
43	SO$_3$Na	4-fluoro-3-methoxy	43	464.40	624	Blue	99.3
44	SO$_3$Na	4-chloro-3-methoxy	40	480.85	624	Blue	99.7
49	SO$_3$Na	2-carboxy-3-fluoro	40	478.38	594	Blue	98.0
52	SO$_3$Na	2-carboxy-4-hydroxy	68	476.39	630	Blue	100.0
53	SO$_3$Na	2-carboxy-4-nitro	21	505.39	584	Blue	95.7

Structure B

58	SO$_3$Na	4-fluorophenoxy	41	526.47	630	Blue	99.5
59	SO$_3$Na	4-chlorophenoxy	25	542.92	630	Blue	98.6
60	SO$_3$Na	4-bromophenoxy	17	587.38	625	Blue	96.1
61	SO$_3$Na	2,4-dimethylphenylthio	10	552.59	640	Blue	96.1
62	SO$_3$Na	2,5-dimethylphenylthio	7	552.59	640	Blue	98.0
63	SO$_3$Na	3,4-dimethylphenylthio	7	552.59	640	Blue	95.9
64	SO$_3$Na	3-pyridylmethylthio	14	539.56	640	Blue	98.6

Structure C

68	SO$_3$H	fluoro	97	397.38	500	Purple	98.5
69	SO$_3$H	methoxy	38	409.41	506	Purple	95.2

[a]Isolated yield; [b]Purity of the compounds was determined using LC-MS coupled to a diode array detector (220-900 nm).

Purification of Reactive Blue 2. RB-2 has been used since decades as a valuable pharmacological tool for studying nucleotide receptors. Most studies relied on commercially available products. However, there has always been some doubt regarding the identity and purity of commercial products, making it difficult to obtain reliable pharmacological results.[41–43] RB-2 is a mixture of two isomers bearing a sulfonate group either in position 3 or 4 of ring F (compound **2**, Figure 1). Thus, we decided to investigate the purity of commercially available RB-2. The purity of the investigated RB-2 was declared to be 88.2 % as determined by HPLC-UV. However, the employed technique is not suitable to detect inorganic impurities, e.g. inorganic salts. Therefore, we purified commercially available RB-2 by reversed phase-18 flash column chromatography (RP-18 FCC, for details see experimental section). Subsequent analysis showed that the commercial product only contained 54 % of RB-2, while the main organic contaminant was found to be the precursor of RB-2, namely disodium 1-amino-4-[4-(4,6-dichloro-[1,3,5]triazin-2-ylamino)-3-sulfonatophenylamino]-9,10-dioxo-9,10-dihydroanthracene-2-sulfonate (ca. 12 %). Moreover, it was found to be contaminated with ca. 34 % of inorganic salts, presumably NaCl and Na$_3$PO$_4$, which were washed out during the purification step using RP-18 column chromatography.

Biological assays. The potencies of the compounds were determined using a fluorescence–based Ca^{2+}-mobilization assay according to the following principle: monoclonal colonies of 1321N1 astrocytoma cells stably transfected with the human P2Y$_4$ receptor were loaded with

the acetoxymethyl ester of the calcium-sensitive fluorescent dye fluo-4. The $P2Y_4$ receptor is coupled to G_q protein. Thus, receptor activation with the endogenous ligand UTP will lead to an increase in the intracellular calcium ion concentration and a rise in the intensity of fluorescent light emitted by the dye. Test compounds that act as $P2Y_4$ receptor antagonists inhibit the increase in fluorescence intensity, which is monitored using a microplate fluorescence reader. Prior to evaluating the antagonistic activity of the anthraquinone derivatives, a concentration-response curve of the agonist UTP at the human $P2Y_4$ receptor was obtained (Figure 2). The EC_{80} of UTP at this cell line was determined to be 565 nM. A UTP concentration of 500 nM, close to its EC_{80} value, was subsequently used for receptor activation for the determination of antagonist potency using the calcium mobilization assay.

A total of 64 synthesized anthraquinone derivatives including 21 new compounds not previously described in literature along with the commercially obtained and the purified RB-2 were tested for their inhibitory activity at the human $P2Y_4$ receptor. The IC_{50} values are summarized in Tables 2-4.

Structure–activity relationships. Purified RB-2 (**2'**) displayed an IC_{50} value of 0.625 µM and hence was more potent than the commercially available RB-2 (IC_{50} = 1.14 µM, Figure 3 and Table 1). This is very reasonable, since the dye content of commercially available RB-2 was found to be only 54 %. While the hill slope of the concentration-inhibition curve for purified RB-2 (**2'**) was found to be close to unity, crude RB-2 had a much steeper hill slope of -2.20. This might be due to allosteric modulatory effects of the contaminants present in the non-purified material, e.g., inorganic salts.[44]
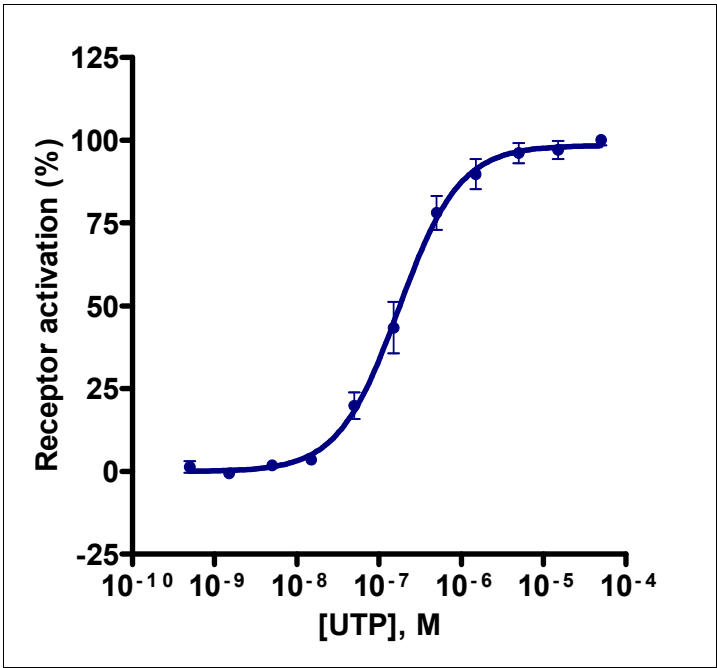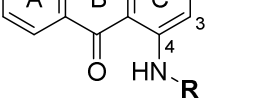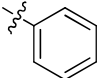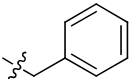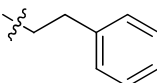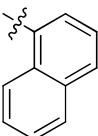
Figure 2. Concentration-response curve of the agonist UTP determined by calcium-mobilization assays on recombinant 1321N1 astrocytoma cells stably expressing the human $P2Y_4$ receptor. Data points shown are the mean values of eight independent experiments, each performed in duplicates. The determined EC_{50} of UTP is 203 ± 41 nM. The calculated EC_{80} value is 565 nM.
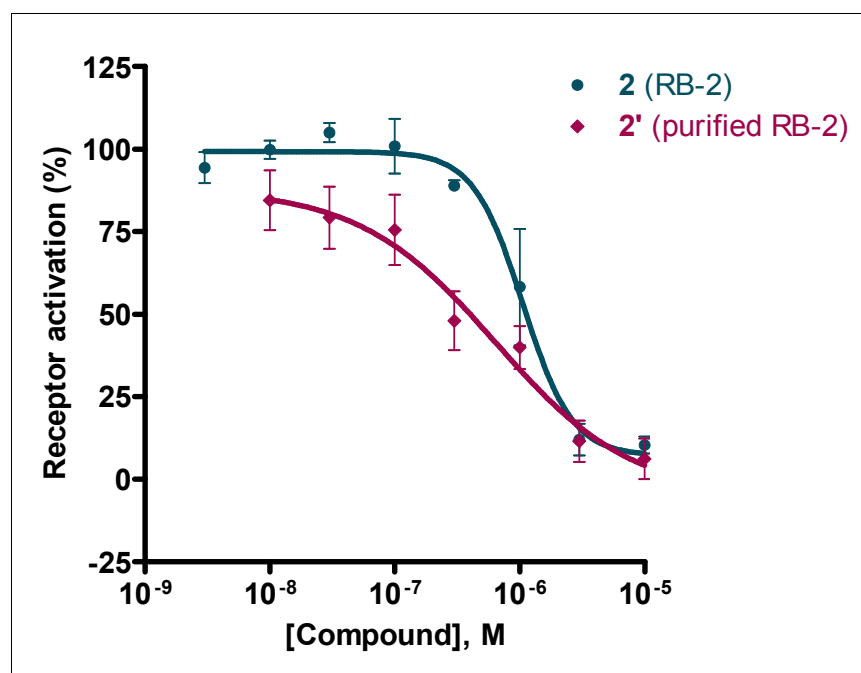
Figure 3. Concentration-response curves of the commercially available RB-2 (**2**) and purified RB-2 (**2'**), determined using the calcium-mobilization assay on recombinant 1321N1 astrocytoma cells stably expressing the human $P2Y_4$ receptor. UTP at a concentration of 500 nM (~EC_{80}) was used for receptor activation. Data points shown are the mean values of at least three independent experiments, each performed in duplicates. The IC_{50} values are **1.14** ± 0.31 for the commercially available RB-2 (**2**), Hill slope -2.20, and **0.625** ± 0.198 for the purified RB-2 (**2'**), Hill slope -0.80.

Regarding the synthesized compounds, the structurally simple 1-amino-4-phenylamino-2-sulfoanthraquinone, Acid Blue-25 (AB-25, **7**), showed inhibitory activity at low micromolar concentrations (IC_{50} = 3.10 µM), being almost as potent as the much larger RB-2 (IC_{50} = 1.14 µM). Replacing the phenylamino ring by benzylamino, phenethylamino, or α-naphthylamino (**8–10**) decreased the activity by more than two-fold (Table 2).

Table 2. Antagonistic Activity of Anthraquinone Derivatives at the Human P2Y$_4$ Receptor –
Part I
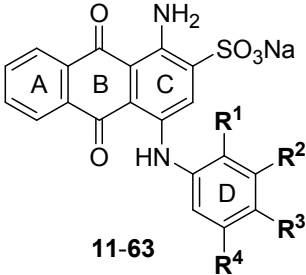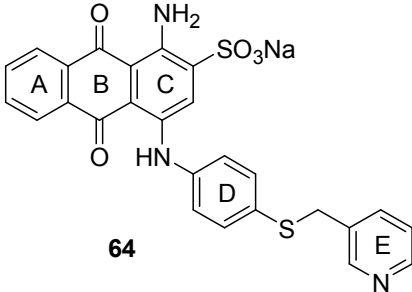
Compound	R	IC$_{50}$ ± SEM (μM)^a
7		3.10 ± 0.35
8		14.4 ± 3.50
9		7.18 ± 0.80
10		7.42 ± 2.77
2 (RB-2)	For structure see Figure 1	1.14 ± 0.31
2' (RB-2 purified)	For structure see Figure 1	0.625 ± 0.198

^{a}Potency to inhibit calcium mobilization following receptor activation with 500 nM UTP (EC$_{80}$) in 1321N1 astrocytoma cells stably transfected with the human P2Y$_4$ receptor.

These results suggested that a phenylamino substituent at the 4-position of the anthraquinone core structure is preferred for P2Y$_4$ receptor inhibitory potency over a benzyl or phenethyl residue. Therefore, a library consisting of 60 derivatives of lead structure **7** with various *mono-* and *di-*substitutions on the phenyl ring attached to the 4-amino group was investigated for inhibitory potency at the P2Y$_4$ receptor (see Table 3).

Table 3. Antagonistic Activity of Anthraquinone Derivatives at the Human $P2Y_4$ Receptor –

Part II

Compound	R^1	R^2	R^3	R^4	$IC_{50} \pm SEM$ $(\mu M)^a$ (or % inhibition at indicated concentration)
11	F	H	H	H	**1.97** ± 0.42
12	H	F	H	H	**1.39** ± 0.36
13	H	H	F	H	**4.04** ± 1.01
14	Cl	H	H	H	**9.34** ± 2.07
15	H	Cl	H	H	**2.34** ± 0.71
16	H	H	Cl	H	**3.03** ± 0.66
17	H	Br	H	H	**6.96** ± 0.73
18	H	H	Br	H	**3.30** ± 0.09
19	CH_3	H	H	H	**3.49** ± 0.29
20	H	CH_3	H	H	**2.22** ± 0.31
21	H	H	CH_3	H	**2.82** ± 0.92
22	C_2H_5	H	H	H	**3.53** ± 1.21
23	H	C_2H_5	H	H	**1.51** ± 0.48
24	H	H	C_2H_5	H	**3.21** ± 0.91
25	H	C_3H_7	H	H	**2.99** ± 0.12
26	OMe	H	H	H	**3.98** ± 1.39
27	H	OMe	H	H	**1.70** ± 0.24

28	H	H	OMe	H	2.59 ± 0.72
29	H	H	OH	H	3.16 ± 0.58
30	CO_2H	H	H	H	6.10 ± 1.72
31	H	CO_2H	H	H	23.4 ± 3.6
32	H	H	CO_2H	H	$\approx 30\ (57\ \%)^b$
33	CH_3	CH_3	H	H	2.63 ± 0.59
34	CH_3	H	CH_3	H	3.58 ± 0.25
35	CH_3	H	H	CH_3	11.2 ± 1.20
36	H	CH_3	H	CH_3	6.45 ± 2.22
37	H	OMe	OMe	H	4.98 ± 0.99
38	H	OMe	H	OMe	9.25 ± 4.56
39	H	OMe	CH_3	H	4.13 ± 0.99
40	CH_3	H	Cl	H	2.20 ± 0.52
41	H	CH_3	Cl	H	1.65 ± 0.37
42	H	CH_3	OH	H	0.746 ± 0.076
43	H	OMe	F	H	1.54 ± 0.66
44	H	OMe	Cl	H	3.37 ± 1.09
45	H	F	H	F	12.5 ± 2.30
46[14]	CO_2H	H	F	H	$> 100\ (17\ \%)^c$
47	CO_2H	H	Cl	H	$> 100\ (31\ \%)^c$
48	CO_2H	H	Br	H	$> 100\ (30\ \%)^b$
49	CO_2H	F	H	H	$> 100\ (10\ \%)^c$
50	CO_2H	H	H	F	$> 100\ (33\ \%)^c$
51	CO_2H	H	H	Cl	2.76 ± 0.75
52	CO_2H	H	OH	H	21.1 ± 7.1
53	CO_2H	H	NO_2	H	$> 30\ (30\ \%)^b$
54	H	H	benzyl	H	3.45 ± 0.41
55	H	H	phenoxy	H	1.94 ± 0.54

56	H	H	phenylamino	H	**1.91 ± 0.28**
57	H	H	phenylthio	H	**1.18 ± 0.09**
58	H	H	4-fluorophenoxy	H	**1.69 ± 0.38**
59	H	H	4-chlorophenoxy	H	**0.373 ± 0.112**
60	H	H	4-bromophenoxy	H	**1.76 ± 0.49**
61	H	H	2,4-dimethylphenylthio	H	**0.233 ± 0.079**
62	H	H	2,5-dimethylphenylthio	H	**0.395 ± 0.082**
63	H	H	3,4-dimethylphenylthio	H	**0.482 ± 0.137**
64			see structure above		**0.409 ± 0.138**

[a]Potency to inhibit calcium mobilization following receptor activation with 500 nM UTP (EC_{80}) in 1321N1 astrocytoma cells stably transfected with the human $P2Y_4$ receptor. [b]% Inhibition at 30 µM. [c]% Inhibition at 100 µM.

Introducing different lipophilic substituents in the *ortho*-, *meta*-, and *para*-positions in ring D, e.g. a halogen atom (F, Cl, Br), an alkyl (CH_3, C_2H_5, C_3H_7), or a methoxy group, did not alter the activity, which ranged between 1 and 9 µM (compounds **11**-**28**, Table 3). On the other hand, introducing hydrophilic moieties led to a reduction in potency by over a ten-fold in the case of *meta*- and *para*-carboxy, while *ortho*-carboxy and *para*-hydroxy substitutions were tolerated (compounds **29**-**32**, Table 3).

In the next step, we assessed *di*-substitution in ring D (Table 3): *di*-substitution with lipophilic residues did not alter the compounds' potency (compounds **33**-**41** and **43**-**45**, Table 3). However, a combination of lipophilic and hydrophilic substituents affected the activity in three different directions: 3-methyl-4-hydroxy (**42**; IC_{50} = 0.746) enhanced the antagonistic activity by over four-fold, 2-carboxy-5-chloro (**51**; IC_{50} = 2.76) was tolerated, whereas any other combination, 2-carboxy-4-fluoro (**46**), 2-carboxy-4-chloro (**47**), 2-carboxy-4-bromo (**48**), 2-carboxy-3-fluoro (**49**), 2-carboxy-5-fluoro (**50**), 2-carboxy-3-hydroxy (**52**), and 2-carboxy-3-nitro (**53**), dramatically decreased the inhibitory activity up to over a hundred-fold (Table 3).

In order to investigate the effect of the presence of an additional ring E, eleven new compounds (**54-64**) were synthesized. In the first step, different bridges (CH_2, O, NH, S) in the *para*-position of ring D were investigated. All four linkers were tolerated (compounds **54-57**, IC_{50} = 3.45, 1.94, 1.91, and 1.18 µM, respectively, Table 3). In the next step, different substituent were introduced into ring E, including halogen (F, Cl, Br) and methyl groups. 4-fluorophenoxy and 4-bromophenoxy residues were found to have no influence on the antagonistic activity (compounds **58** and **60**, IC_{50} = 1.69 and 1.76, respectively, Table 3), while 4-chlorophenoxy substitution increased the potency by > eight-fold (**59**, IC_{50} = 0.373). *Di*-methylation in ring E with a sulfide linker between ring D and E improved potency by more than 13-fold (compounds **61-64**, IC_{50} = 0.233, 0.395, 0.482, and 0.409 µM, respectively, Table 3 and Figure 4). Indeed, compound **61** (IC_{50} = 0.233 µM) can be considered as the most potent $P2Y_4$ receptor antagonist known to date.

As a next step, we were interested in investigating the effects of other substituents on the anthraquinone core, namely the amino group in the 1-position and the sulfonate group in the 2-position. Therefore, we developed six new analogs (**65-70**, Table 4) of selected anthraquinone derivatives (**12**, **27**, and **46**). No improvement in the activity of compound **46** (IC_{50} > 100, Table 3) was observed upon replacement of the sulfonate group with a methyl group (compound **67**) or upon deamination at the 1-position (compound **70**). Moreover, replacement of the 2-sulfonate group of compounds **12** and **27**, (IC_{50} = 1.39 and 1.70 µM, respectively, Table 3) with a methyl group completely abolished the activity (compounds **65** and **66**, respectively, Table 4). Similar results were obtained with the de-aminated compounds **68** and **69** (Table 4). These results indicate that the presence of an amino group in the 1-position and a sulfonate function in the 2-position of the anthraquinone core are essential for antagonistic activity at the $P2Y_4$ receptor.
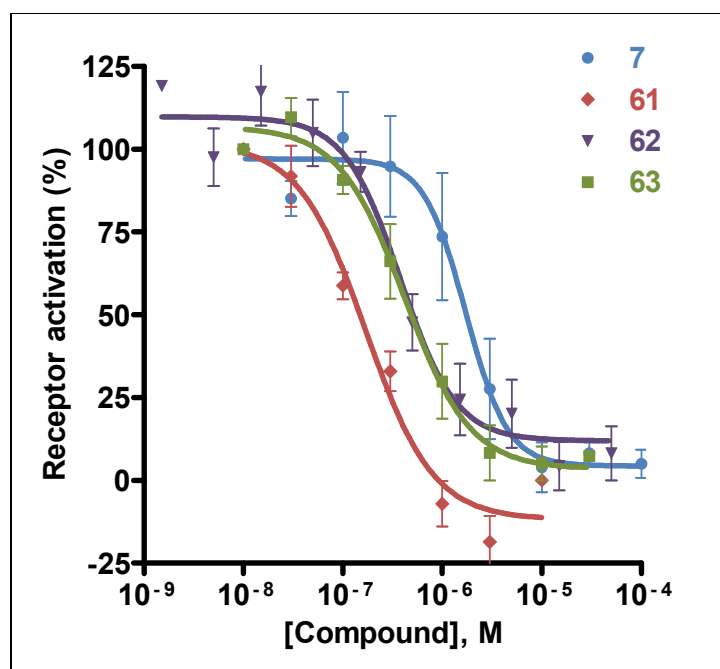
Figure 4. Concentration-response curves of selected anthraquinone derivatives, determined using the calcium mobilization assay with recombinant 1321N1 astrocytoma cells stably expressing the human P2Y$_4$ receptor. UTP at a concentration of 500 nM (EC$_{80}$) was used for receptor activation. Data points shown are the mean values of at least three independent experiments, each performed in duplicates. The IC$_{50}$ values are found in Tables 2 and 3.

Table 4. Inhibitory Potencies at the Human P2Y$_4$ Receptor of Selected Anthraquinone Derivatives Modified in the 1- and 2-Positions.

	Structure A			
Compound	**R^1**	**R^2**	**R^3**	**IC$_{50}$ ± SEM (μM)^a** (or % inhibition at indicated concentration)
Structure A				
12	H	F	H	**1.39 ± 0.36**
27	H	OMe	H	**1.70 ± 0.28**
46	CO$_2$H	H	F	> 100 (17 %)^c
Structure B				
65	H	F	H	> 30 (-4 %)^b
66	H	OMe	H	> 30 (38 %)^b
67	CO$_2$H	H	F	≈ 100 (57 %)^c
Structure C				
68	H	F	H	≈ 30 (49 %)^b
69	H	OMe	H	> 10 (77 %)^b
70	CO$_2$H	H	F	> 100 (25 %)^c

^{a}Potency to inhibit calcium mobilization following receptor activation with 500 nM UTP (EC$_{80}$) in 1321N1 astrocytoma cells stably transfected with the human P2Y$_4$ receptor; ^{b}% Inhibition at 30 μM; ^{c}% Inhibition at 100 μM

Comparison of structure-activity relationships of anthraquinone derivatives at different targets. An overview of the structure-activity relationships (SARs) of the investigated anthraquinone derivatives at the human P2Y$_4$ receptor is depicted in Figure 5. The ABCDE

aromatic ring system proved to be important for high inhibitory potency. The amino function in the 1-position and the sulfonate group in the 2-position of the anthraquinone scaffold were found to be essential for the activity. This is in accordance with previous studies on the SARs of RB-2 and related dyes, which showed that AB-25 is the minimum structural requirement for biological activity of this class of compounds.[24,29,30,33,45–52] Moreover, the activity on the P2Y$_4$ receptor was strongly affected by the substituents present on ring E, e.g. a lipophilic substitution in the *ortho*-, *meta*-, or *para*-position increased the activity, while an unsubstituted ring E with an -SCH$_2$-linker was also tolerated.
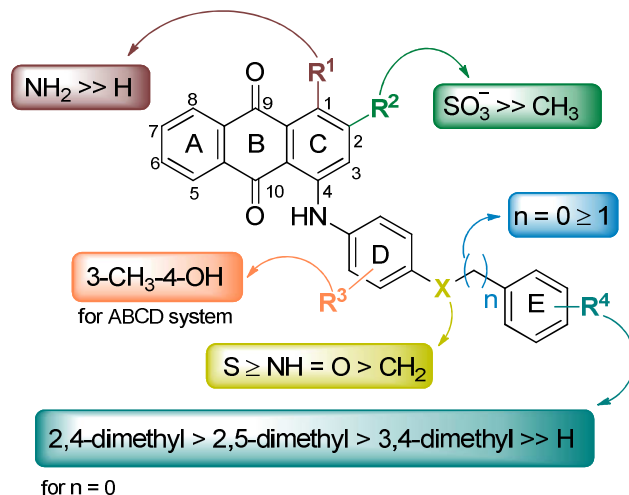
Figure 5. Summary of structure-activity relationships of anthraquinone derivatives as P2Y$_4$ receptor antagonists.

It is interesting to compare the results of the SAR analysis at the human P2Y$_4$ receptor with that at other purinergic targets (Figure 53, Supplementary material). The main difference between the human P2Y$_4$ receptor and both the human P2Y$_{12}$ receptor and P2Y$_1$-like receptors of the guinea-pig taenia coli (receptor was not cloned but found to be pharmacologically similar to the recombinant P2Y$_1$-receptor subtype)[41] is that substitution of

ring D with a sulfonate group at the *meta*-position (for P2Y$_{12}$ receptors)[29,37] and at the *ortho*-position (for the P2Y$_1$-like receptors) was essential for the inhibitory activity of the compounds. An additional ring F was also important in case of the P2Y$_1$-like receptor.[32,42] For activity at the AMP-hydrolyzing enzyme *ecto*-5'-nucleotidase, ring system ABCD was sufficient for the inhibitory activity.[24] In contrast, a triazine or pyrimidine as ring E was preferred by the P2X2 receptor.[31] On the other hand, development of anthraquinone compounds as large conductance Ca^{2+}-activated K$^+$ channel openers showed a preference for a bulky and hydrophobic ring D.[53] Interestingly, the amino group at ring C was not essential for activity at that target.[53]

These differences in SARs emphasize the influence of the nature of substituents at the 4-position of the anthraquinone ring on the potency and target-selectivity of the compounds, and allow the development of receptor (subtype)-selective ligands.

Selectivity. To gain insights into the selectivity of these compounds, we assessed the most potent compounds of this series, **61-64**, on the receptor subtypes that share the greatest sequence homology with the P2Y$_4$ receptor, namely P2Y$_1$, P2Y$_2$, and P2Y$_6$, which belong to the subgroup of G$_q$ protein-coupled P2Y$_1$-like P2Y receptors. In addition, we investigated selected compounds at the P2Y$_{12}$ receptor that had previously been shown to be potently blocked by anthraquinone derivatives.[30] Table 5 and Figure 6 summarize the results. Of this series of compounds, **64** is the most selective one, with particularly high selectivity versus the P2Y$_1$ and P2Y$_6$ receptors, where it showed only low potency. Selectivity against the P2Y$_{12}$ receptor was also observed. It can therefore be concluded that these compounds display P2Y$_4$ receptor selectivity, and it is not only the potency, but also the selectivity of lead structure **7** that has been significantly enhanced (see Figure 6).
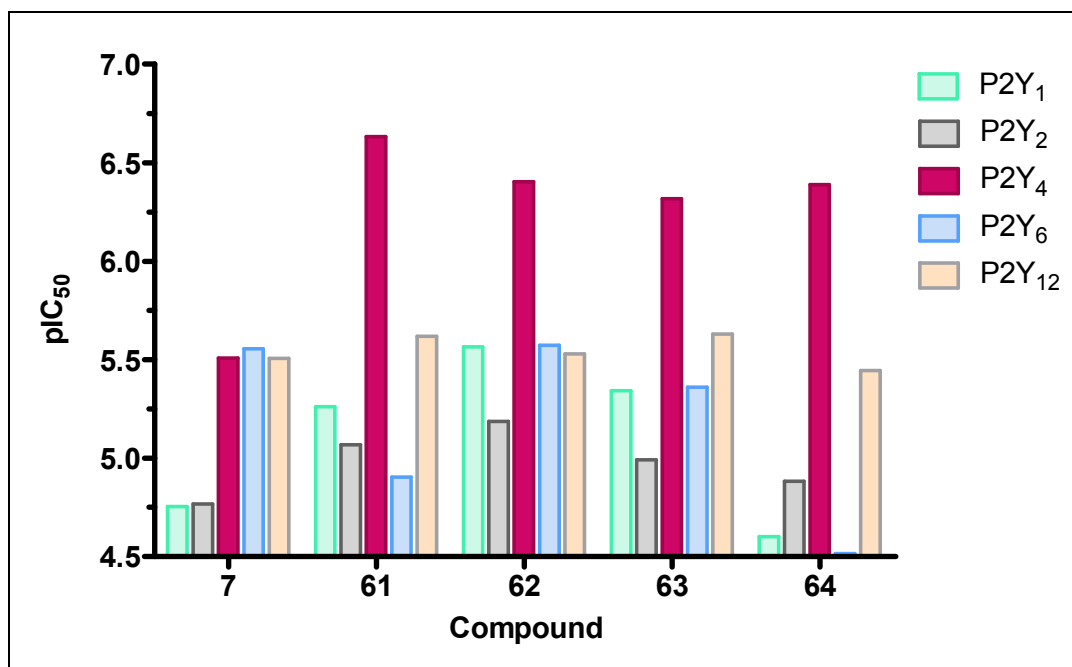
Figure 6. Potency of selected anthraquinone derivatives on different human P2Y receptors determined using the calcium mobilization assay (P2Y$_{1-6}$ receptors) or β-arrestin translocation assay (P2Y$_{12}$ receptor). Shown are the pIC$_{50}$ values of at least three independent experiments performed in duplicates.

Table 5. Selectivity of the Most Potent P2Y$_4$ Receptor Antagonists versus Other P2Y Receptor Subtypes[a]

Compd	R	IC$_{50}$ ± SEM (µM) or (% Inhibition at 50 µM)				
		hP2Y$_4$	**hP2Y$_1$**	**hP2Y$_2$**	**hP2Y$_6$**	**hP2Y$_{12}$**
7	H	**3.10** ± 0.35	**17.6** ± 6.5	**17.1** ± 6.3	**2.79** ± 0.17	**3.12** ± 1.17
42	3-methyl-4-hydroxy	**0.746** ± 0.076	**7.65** ± 1.90	**16.4** ± 4.5	**4.75** ± 1.49	**0.0604** ± 0.0147
61	2,4-dimethyl	**0.233** ± 0.079	**5.48** ± 0.34	**8.54** ± 1.45	**12.5** ± 3.9	**2.41** ± 0.45
62	2,5-dimethyl	**0.395** ± 0.082	**2.72** ± 0.59	**6.52** ± 1.04	**2.67** ± 0.91	**2.96** ± 0.24
63	3,4-dimethyl	**0.482** ± 0.137	**4.55** ± 0.42	**10.2** ± 1.5	**4.36** ± 0.60	**2.34** ± 0.10
64	see structure above	**0.409** ± 0.138	~ 25 (61 ± 4 %)	**13.1** ± 2.6	>> 100 (12 ± 19 %)	**3.59** ± 0.38

[a]Potency to inhibit calcium mobilization in 1321N1 astrocytoma cells recombinantly expressing human P2Y recetors following receptor activation with 500 nM ADP (P2Y$_1$), 500 nM UTP (P2Y$_2$, P2Y$_4$), or 750 nM UDP (P2Y$_6$). Potency at the G$_i$-coupled P2Y$_{12}$ receptor was determined using a β-arrestin translocation assay.

The binding mode of anthraquinone derivatives at the P2Y$_4$ receptor. The mode of antagonism, competitive or non-competitive, at the P2Y$_4$ receptor was determined using the most potent compound (**61**) of the present series. Concentration-response curves of the endogenous ligand UTP after a pre-incubation with fixed concentrations of **61** were obtained.

For a competitive antagonist, a parallel rightward shift of the curves towards higher concentrations of UTP would be expected with increasing concentrations of **61**. The upper plateaus of the curves, corresponding to the maximum receptor activation, should remain unaltered. A corresponding Schild plot would show a straight line with a slope of approximately 1. Non-competitive antagonism, on the other hand, is characterized by a suppression of the maximum receptor activation with increasing antagonist concentrations, while the EC_{50} remains largely unaffected. Our results, summarized in Figure 7, show a significant depression of the upper plateaus of the UTP curves with increasing concentrations of **61**. The reduction in the maximum receptor activation is successively more pronounced with rising concentrations of **61**, and a complete blockade of UTP-mediated receptor activation is observed at a concentration of 15 µM of **61**. In the calcium mobilization assay, the cells were first incubated with the antagonist **61** for 30 min. The agonist UTP was subsequently injected into the cell suspension and the assay signal was read immediately thereafter. Since there is no simultaneous incubation with both agonist and antagonist and the measurement of the signal is very fast, the assay conditions are likely to be under non-equilibrium conditions. Nevertheless, our data indicate that **61** may achieve $P2Y_4$ receptor antagonism via a non-competitive mechanism, but competitive antagonism cannot be completely ruled out at present. Interestingly, on the $P2Y_{12}$ receptor, we previously found that anthraquinone derivatives of this series act as competitive antagonists.[30] However, the percentage of sequence shared by the $P2Y_4$ and $P2Y_{12}$ receptors is only 25 % and, consequently, significant differences exist between these two receptors (also with respect to orthosteric ligand preferences and G protein coupling).

In order to get more insight into the interaction of the anthraquinone derivatives with the $P2Y_4$ receptor on a molecular level we decided to perform docking studies.
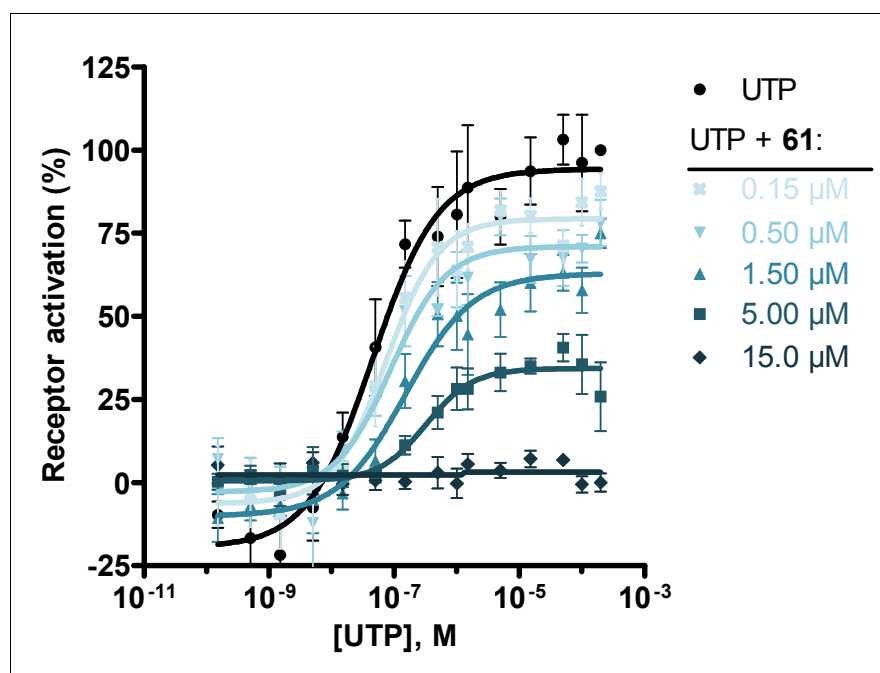
Figure 7. Concentration-response curves of UTP on the P2Y$_4$ receptor after pre-incubation with fixed concentrations of **61**. The results were obtained using the calcium-mobilization assay with 1321N1 astrocytoma cells recombinantly expressing the human P2Y$_4$ receptor. EC$_{50}$ values are not significantly different from each other ($p > 0.05$, unpaired t-test). The EC$_{50}$ values and maximum receptor activation are shown in the Supplementary material.

Analysis of the human P2Y$_4$ receptor model. Two P2Y receptor subtypes, the more distantly related P2Y$_{12}$ and the more closely related P2Y$_1$ receptors, had been crystallized and X-ray structures were obtained in complex with agonists (P2Y$_{12}$) and antagonists (P2Y$_1$, P2Y$_{12}$).[54–56] Based on these structures, the molecular mechanism of activation of the human P2Y$_1$ receptor was recently analyzed by molecular dynamics simulations, which explained the essential role of the amino acids Asp204 in extracellular loop 2 (ECL2) and Arg310 in the transmembrane region 7 (TM7).[57] The two amino acids Asp204 and Arg310 form an ionic lock and are stabilized in the inactive state by P2Y$_1$ antagonists. The ionic lock is broken

during the activation of the receptor by the agonist adenosine diphosphate (ADP). We constructed a homology model of the $P2Y_4$ receptor based on the $P2Y_1$ receptor. In our inactive state homology model of the human $P2Y_4$ receptor, an ionic lock between Asp187 and Arg292 was formed, suggesting a similar mechanism of activation as in the human $P2Y_1$ receptor.

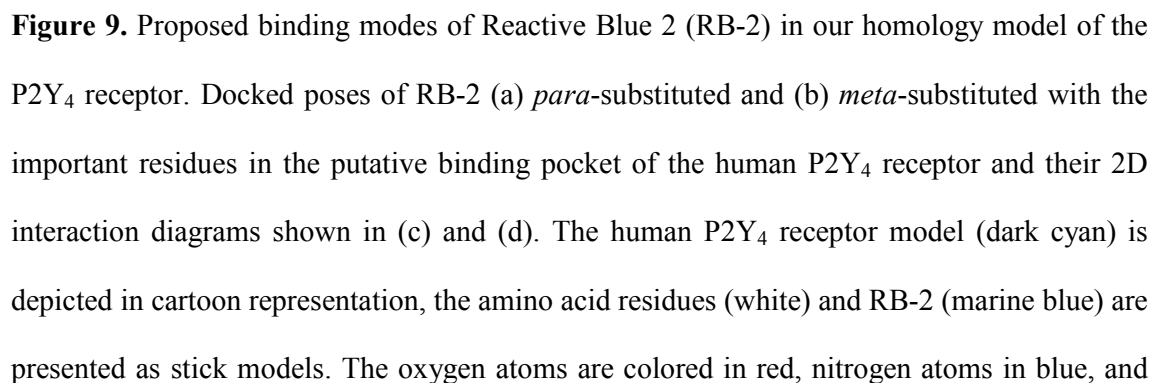Two ligand binding sites located towards the extracellular regions of the $P2Y_4$ receptor were identified in the homology model (Figure 8). The binding site denoted as 'A' with a volume of 190 Å³ was observed upon the downward movement of the ECL2. This binding site 'A' is comparable to the binding site of the non-competitive antagonist 2-iodo-N^6-methyl-(*N*)-methanocarba-2'-deoxyadenosine-3',5'-bisphosphate (MRS2500, **72**) in the human $P2Y_1$ receptor with a size of 214 Å³. The second binding site in the homology model of the $P2Y_4$ receptor, denoted as 'O', is formed in the region comparable to the orthosteric binding site identified in the crystal structure of the human $P2Y_{12}$ receptor in complex with the agonist 2-methylthioadenosine-5'-diphosphate (2MeSADP, **71**), and in the molecular dynamics simulation study of the human $P2Y_1$ receptor with the agonist ADP.[56,57] In our inactive state model of the human $P2Y_4$ receptor, the binding site 'O' is limited in size due to the downward movement of the ECL2. However, after its upward movement, it could accommodate the endogenous agonists UTP and ATP, respectively. The experimental data for the $P2Y_4$ receptor antagonists developed in this study suggested a non-competitive mode of inhibition. Hence, we selected binding site 'A' for compound docking to probe whether **61** and analogs may display a similar mode of receptor inactivation as MRS2500 (**72**) in the $P2Y_1$ receptor.
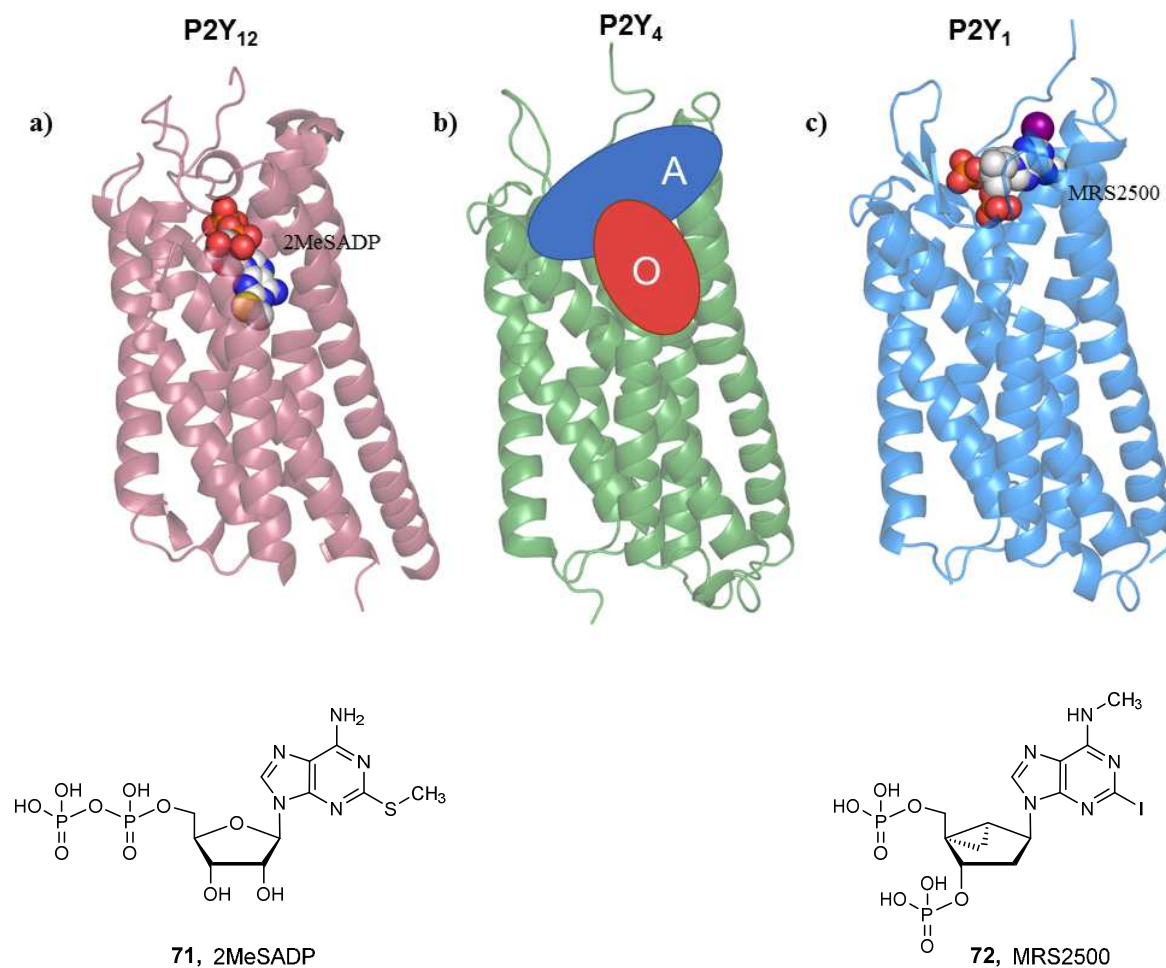
Figure 8. (a) Crystal structure of the human P2Y$_{12}$ receptor (light red) in complex with the agonist 2-methylthio-ADP (2MeSADP, **71**): (b) homology model of the human P2Y$_4$ receptor (light green) with the schematic representation of the orthosteric binding site (denoted 'O') and the allosteric binding site (denoted 'A'); (c) Crystal structure of the human P2Y$_1$ receptor (light blue) in complex with the non-competitive antagonist 2-iodo-N^6-methyl-(*N*)-methanocarba-2'-deoxyadenosine-3',5'-bisphosphate (MRS2500, **72**). The receptors are represented as cartoon models and the small molecules **71** and **72** are represented as space fill models.

Docking studies of Reactive Blue 2 (RB-2). The putative binding modes of the *para-* and *meta*-sulfo-substituted isomers (ring F) of RB-2 are shown in Figure 9. The binding poses showed that the two derivatives have the same orientation in the binding pocket 'A' formed between ECL2 and TM regions V, VI and VII. Ring A of RB-2 appears to be completely exposed to the extracellular space of the human $P2Y_4$ receptor. Ring B may be stabilized by π-π-stacking with Phe29 from the *N*-terminal region of the receptor. The sulfonate group in position 2 of ring C likely binds to Lys179 and Arg272, forming strong electrostatic and hydrogen bonding interactions. The carbonyl groups at positions 9 and 10 of the anthraquinone core, the amino group at position 1, and the amine linker between rings C and D were not observed to form any specific interactions with the amino acids of the human $P2Y_4$ receptor. However, the amino group at position 1 of the anthraquinone ring system probably forms intramolecular H-bond interactions with the carbonyl group at position 9. The sulfonate group at ring D forms strong electrostatic interactions with Lys34, Lys289 and Arg292, and possibly with Asp187 according to our model. Ring E was found to occupy the binding pocket formed by His186 and Thr188 of ECL2, Tyr268 and Arg272 of TM VI, and Tyr288 of TM VII. Ring F is bound by the aromatic residues Tyr116, Tyr197, and Tyr269 between TM regions V and VI. The sulfonate group on ring F (*para-* or *meta*-substituted) interacts with Arg265 through electrostatic interactions and additionally stabilizes the ring in the binding pocket through cation-π interactions as observed for in the docking study.

Figure 9. Proposed binding modes of Reactive Blue 2 (RB-2) in our homology model of the

P2Y$_4$ receptor. Docked poses of RB-2 (a) *para*-substituted and (b) *meta*-substituted with the

important residues in the putative binding pocket of the human P2Y$_4$ receptor and their 2D

interaction diagrams shown in (c) and (d). The human P2Y$_4$ receptor model (dark cyan) is

depicted in cartoon representation, the amino acid residues (white) and RB-2 (marine blue) are

presented as stick models. The oxygen atoms are colored in red, nitrogen atoms in blue, and

sulfur atoms in orange. None of the interacting residues are highly conserved for the subtypes

analyzed in selectivity studies (P2Y$_{1, 2, 4, 6}$, and $_{12}$; see Supplementary Figure 61).

Docking studies of the new, potent P2Y$_4$ antagonists. In order to propose binding modes

for the anthraquinone derivatives that were optimized for P2Y$_4$ receptor blockade, and to

rationalize the determined potency values, we selected compounds **7**, **42** and **61-64** for

performing molecular docking studies on the homology model of the human P2Y$_4$ receptor.

The putative binding pose of the most potent antagonist **61** in the binding pocket and its 2D

interaction diagram are shown in Figure 10. Similar to RB-2, compound **61** can be well

accommodated in binding pocket 'A'. Ring A of **61** faces towards the extracellular space and

rings B and C form hydrophobic interactions with Phe29 and Leu184. The sulfonate group in

ring C could make strong electrostatic interactions with Lys34, Asp187, and Arg292 present

in the pocket formed by Lys34, Tyr94, Asp187, Lys289, and Arg292 of the ECL2 and TMs I,

VI, and VII. Through its strong electrostatic interactions, the sulfonate group may act as an

anchor for the compound and stabilize it in a vertical position through hydrophobic

interactions of ring B and C with Phe29 and Leu184. The carbonyl group at position 9 of the

anthraquinone ring system likely interacts with Asn99 through hydrogen bonding, and the

carbonyl group at position 10 and the amino group at position 1 may form weak hydrogen

bond interactions with Arg272 and Lys34, respectively. Additionally, the amino group at

position 1 of the anthraquinone probably forms intramolecular interactions with the carbonyl

group at position 9 and the sulfonate oxygen at ring C. The importance of the amino group at

position 1 was confirmed for compounds **68-70** by replacing the amino group with a hydrogen

atom. This led to a significant drop in inhibitory potency. The amine linker between ring C

and D may form weak hydrogen bond interactions with His186. We hypothesize that the

sulfonate group at ring C forms strong electrostatic interactions with Arg292, it is essential for

high potency of the anthraquinone derivatives. Replacement by a carboxylic acid group

decreased potency (see **30-32**, **46**, **67**, and **70**). A possible explanation is that both acidic structures compete for the same binding subpocket interacting with Arg292, which might lead to different binding modes. Furthermore, the binding pocket of ring D appears to be limited in space with the subpocket formed by His186, Thr188 of ECL2 and Tyr268, Arg272, and Tyr288 of TMs VI and VII. In this pocket, phenyl substitutions are well tolerated, as opposed to the bulky naphthyl group (compounds **8-10**). This was additionally supported by the linker preferences between ring D and E: S > O > NH > CH$_2$. Thiophenoxy derivatives were most potent, likely because the orientation provided by a sulfur linker is required for positioning ring E into the hydrophobic pocket. Except for compound **62**, ring D of the docked compounds showed the same orientation within the subpocket (Supplementary Figure 54).

a)

b)

c)
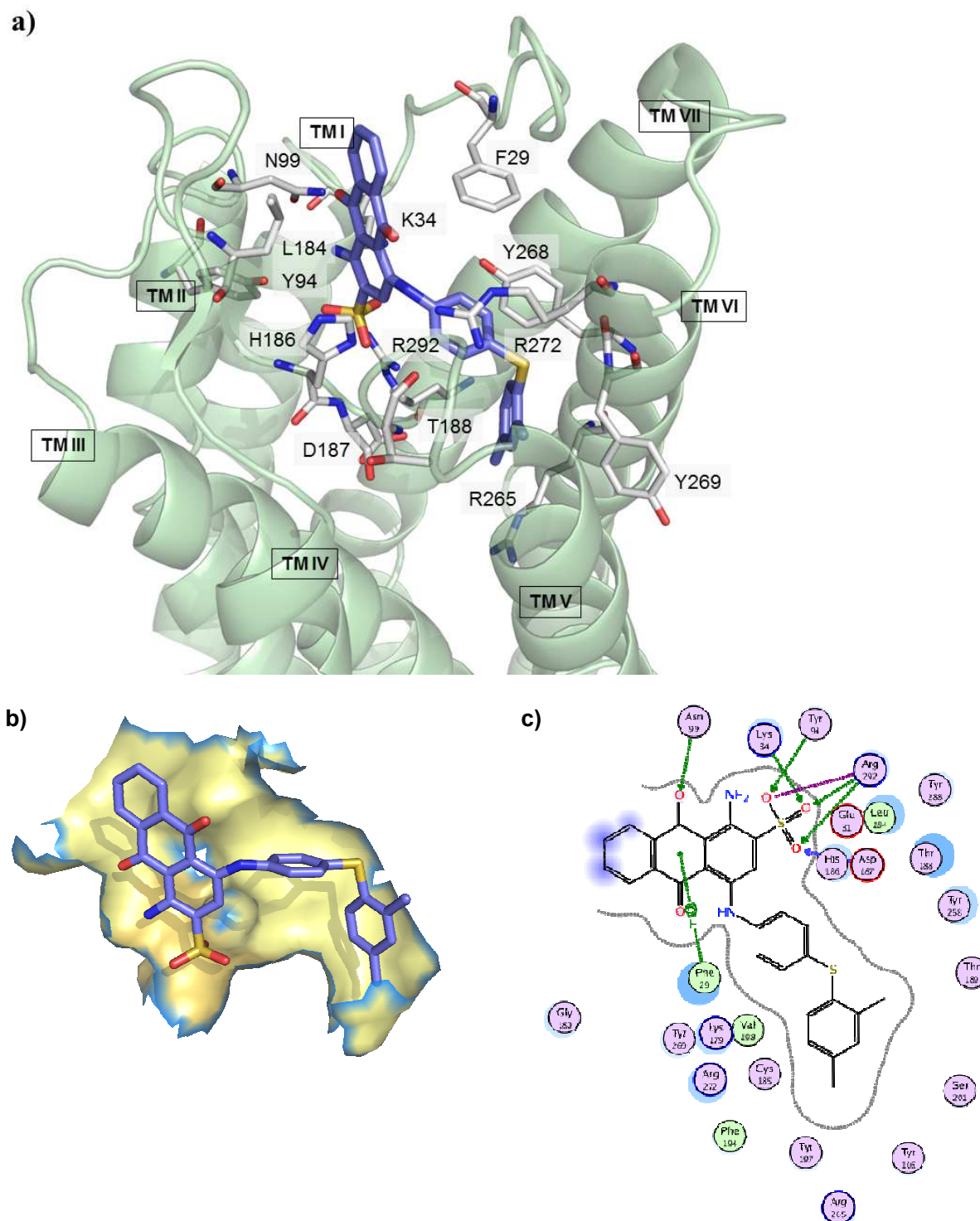
Figure 10. Proposed binding mode of **61** in our homology model of the P2Y$_4$ receptor. (a)

docked pose of **61** with the important residues in the putative binding pocket of the human

P2Y$_4$ receptor; (b) the putative binding pocket is shown in a surface model; the 2D interaction

diagrams are shown in (c) and (d). The human P2Y$_4$ receptor model (dark cyan) is displayed

in cartoon representation, the amino acid residues (white) and compound **61** (marine blue) are

shown as stick models. The oxygen atoms are colored in red, nitrogen atoms in blue, and

sulfur atoms in orange. As for RB-2, none of the residues interacting with **61** are highly

conserved for the subtypes analyzed in selectivity studies (P2Y$_{1, 2, 4, 6}$, and $_{12}$; see

Supplementary Figure 61).

The terminal ring E present in **61-63** and **64** was found to occupy the pocket formed by

Tyr116 of TM III, Phe194, Tyr197, and Val198 of TM V, and Arg265, Tyr268, and Tyr269 of

TM IV. Due to a large number of aromatic residues, compounds with a ring E may be tightly

packed within the pocket, resulting in somewhat improved potency in comparison to the

compounds without ring E. The putative binding modes of compounds **7** and **42** without ring

E and their 2D interaction diagrams are shown in Supplementary Figure 55. The dimethyl

substitutions at ring E are thought to increase the hydrophobic interactions with the aromatic

residues and promote the tight binding of the compound inside the binding pocket of the P2Y$_4$

receptor. Among different substituents, 2,4-dimethylphenylthio-substitution (**61**: 0.233 µM)

showed slightly higher potency as compared to 2,5- and 3,4-dimethylphenylthio-substituted

derivatives (**62**: 0.395 µM; **63**: 0.482 µM). The putative binding poses and 2D interaction

diagrams of **62** and **63** are shown in Supplementary Figure 56. In case of **64**, tight binding was

achieved with an extended linker. Additionally, Arg265 is located at the bottom of the pocket

occupied by ring E and might interact with the pyridine group of **64**. The putative binding

pose and 2D interaction diagram of **64** are shown in Supplementary Figure 57.

As a next step, we compared the binding poses of RB-2 and compound **61** (see overlay of

RB-2 and **61** in Figure 11). Ring B of RB-2 and ring A of **61** form hydrophobic aromatic

interactions with Phe29. The sulfonate groups in ring D of RB-2 corresponds with the

sulfonate group in ring C of **61**; they are believed to interact with Lys34 and Arg292. Ring E

of RB-2 and ring D of **61** occupy the same binding pocket formed by the amino acid residues

His186, Thr188, Tyr268, Arg272, and Tyr288. A comparison of ring F of RB-2 with ring E of

61 shows that the sulfonate group in ring F probably displays electrostatic interactions with

Arg265 in the bottom part of the hydrophobic pocket. The dimethyl substitution of **61** may

lead to a tightening of the binding pocket through hydrophobic interactions with the aromatic

residues instead. Thus, our homology model explains the positive contributions of lipophilic

terminal moieties on the anthraquinone derivatives as well as those of a polar sulfonate moiety

as in RB-2.
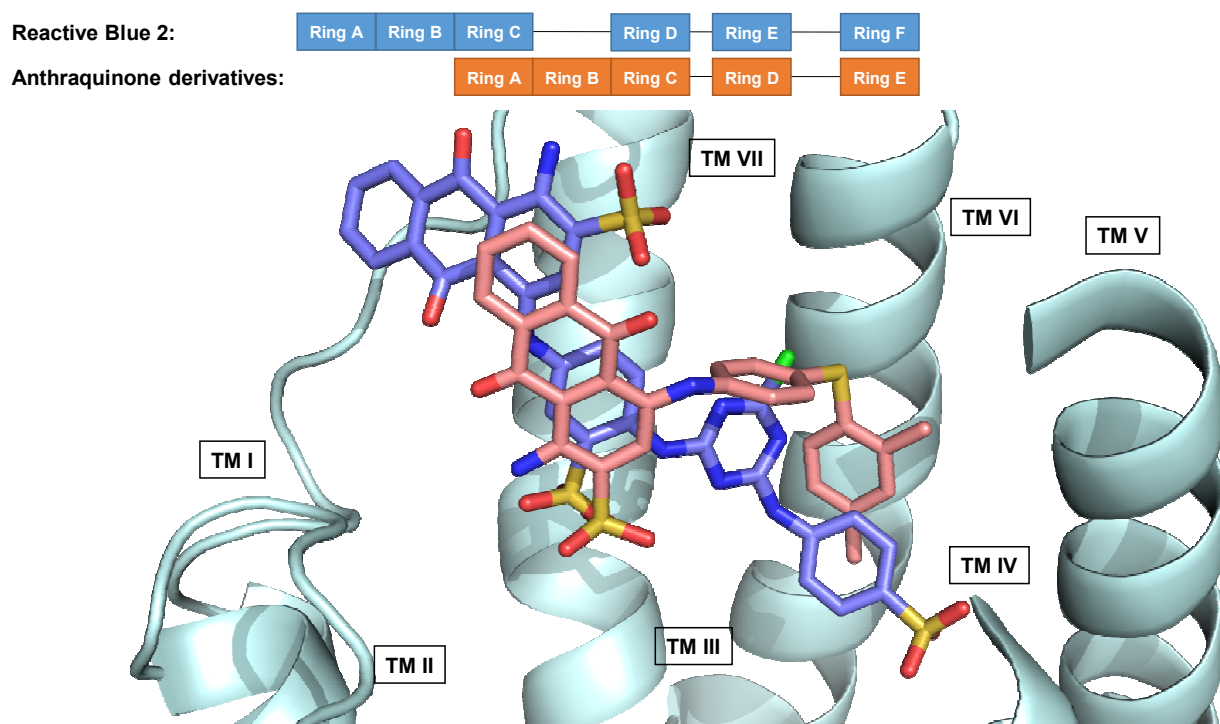
Figure 11. Comparative overlay of the docked poses of *para*-substituted RB-2 (in blue) and

compound **61** (in red) in the binding pocket of the human P2Y$_4$ receptor model. The overlap

of the ring system of RB-2 and **61** is shown in the schematic representation on the top.

A further important observation regarding the binding poses of the antagonists in the binding pocket of the human $P2Y_4$ receptor relate to the orientation and interactions of Asp187 and Arg292, which correspond to Asp204 and Arg310 in the human $P2Y_1$ receptor. This supports the hypothesis that the mode of $P2Y_4$ receptor inhibition by anthraquinone derivatives is similar to that described for **72** at the $P2Y_1$ receptor. They stabilize the ionic lock and prevent the movement of TMs VI and VII required for receptor activation. Our docking results are consistent with the experimental data and the SARs of anthraquinone derivatives. The homology model of the human $P2Y_4$ receptor will be useful for future compound optimization and allow rational ligand design and virtual screening approaches.

Conclusions

In conclusion, we have synthesized a library of RB-2-related anthraquinone derivatives and successfully optimized them as selective antagonists of the human $P2Y_4$ receptor. To the best of our knowledge, compound **61** (sodium 1-amino-4-[4-(2,4-dimethylphenylthio)-phenylamino]-9,10-dioxo-9,10-dihydroanthracene-2-sulfonate) represents the most potent $P2Y_4$ receptor antagonist known to date, with an IC_{50} value of 233 nM. Our results suggest that **61** exerts its antagonistic effect on the $P2Y_4$ receptor through a non-competitive mechanism. This was rationalized by the docking of **61** to a homology model of the human $P2Y_4$ receptor based on the recently published X-ray structure of the $P2Y_1$ receptor in complex with allosteric antagonists. As a continuation of our previous work on anthraquinone derivatives, the current results confirm the validity of RB-2 as a privileged structure in the field of purinergic signaling. Furthermore, by fine-tuning the structure, it is possible to develop subtype-specific ligands as valuable pharmacological tool compounds.

Experimental Section

Chemistry

Material and methods. All materials were used as purchased (Acros, Alfa Aesar, Merck, or Sigma-Aldrich, Germany). 3-Propylaniline was prepared according to the method of Rasmussen et al.[58] Thin-layer chromatography was performed using TLC aluminum sheets silica gel 60 F_{254}, or TLC aluminum sheets reversed phase (RP) silica gel 18 F_{254} (Merck, Darmstadt, Germany). Colored compounds were visible at daylight; other compounds were visualized under UV light (254 nm). Flash chromatography was performed on a Büchi system using silica gel RP-18 (Merck, Darmstadt, Germany). ^{1}H- and ^{13}C-NMR data were collected on either a Bruker Avance 500 MHz NMR spectrometer at 500 MHz (^{1}H), or 126 MHz (^{13}C), respectively or a 600 MHz NMR spectrometer at 600 MHz (^{1}H), or 151 MHz (^{13}C), respectively. DMSO-d_6 was used as a solvent. Chemical shifts are reported in parts per million (ppm) relative to the deuterated solvent, i. e. DMSO, δ ^{1}H: 2.49 ppm; ^{13}C: 39.7 ppm, coupling constants J are given in Hertz and spin multiplicities are given as s (singlet), d (doublet), t (triplet), q (quartet), sext (sextet), m (multiplet), br (broad).

The purities of isolated products were determined by ESI–mass spectra obtained on an LC-MS instrument (Applied Biosystems API 2000 LC-MS/MS, HPLC Agilent 1100) using the following procedure: the compounds were dissolved at a concentration of 0.5 mg/mL in H_2O : MeOH = 1 : 1, containing 2 mM NH_4CH_3COO. Then, 10 µL of the sample was injected into an HPLC column (Phenomenex Luna 3µ C18, 50 x 2.00 mm). Elution was performed with a gradient of water : methanol (containing 2 mM NH_4CH_3COO) from 90 : 10 to 0 : 100 starting the gradient immediately at a flow rate of 250 µL/min for 15 min followed by washing with 100 % methanol for another 15 min. UV absorption was detected from 200 to 950 nm using a diode array detector. The purity of the compounds proved to be $\geq$ 95 %. For microwave reactions, a CEM Focused^{TM} Microwave Synthesis type Discover apparatus was used. A

freeze dryer (CHRIST ALPHA 1-4 LSC) was used for lyophilisation. The synthesis and

analysis of compounds **7-12**, **13**, **15-18**, **22**, **23**, **26-32**, **36**, **38**, **45–48**, **50**, **51, 65-67**, and **70**

were previously described.[24,27–29,33,36,38–40] All other compounds (**14**, **19-21**, **24**, **25**, **33-35**, **37**,

39-44, **49**, **52**, **53**, **58-64, 68** and **69**) were newly prepared in analogy to described methods[12–14] with modifications as described below.

Purification of Reactive Blue 2 (RB-2). RB-2 (200 mg) was dissolved in 10 mL of deionized

water and injected into a flash column chromatography type Sepacore® Glass Column C-690

(ID 26x500 mm) two-thirds filled with reversed phase-18 silica gel (40-63 µm, Merck) using

water as eluent. The polarity was gradually decreased by increasing the concentration of

methanol (5, 10, 20, 40, and 60 %). The pooled blue colored fractions were collected and

evaporated under vacuum to remove the methanol, and the remaining water was subsequently

removed by lyophilization to yield 108 mg (54 %) of RB-2 P (**2'**) as a blue powder. The

chemical structure and purity were confirmed by RP-TLC, LC-MS (> 96 %), and NMR.

General procedure A. Preparation of 4-substituted 1-aminoanthraquinone-2-sulfonate

derivatives (14, **19-21**, **24**, **25**, **33-35**, **37**, **39-44**, **49**, **52**, **53**, and **58-64).** To a 5 mL

microwave reaction vial, equipped with a magnetic stirring bar, were added 1-amino-4-bromo

substituted anthraquinone compounds (bromaminic acid sodium salt **6a**) (0.1–0.3 mmol) and

the appropriate aniline or amine derivative (1.5–9.0 eq.), followed by a buffer solution of

Na_2HPO_4 (pH 9.6) (4.5 mL) and NaH_2PO_4 (pH 4.2) (0.5 mL) and a finely powdered elemental

copper (0.002–0.003 g, 5–10 mol %). The mixture was capped and irradiated in the

microwave oven (80–100 W) for 5–24 min at 100–120 °C. Then the reaction mixture was

cooled down to room temperature (rt), and the product was purified using the following

procedure. The contents of the vial were filtered to remove the elemental copper. Then ca. 200

mL of water was added to the filtrate and the aqueous solution was extracted with

dichloromethane (200 mL). The extraction procedure was repeated until the dichloromethane

layer became colorless (2–3 times). Then the aqueous layer was reduced by rotary evaporation

to a volume of 10 – 20 mL, which was subsequently submitted to flash column chromatography using RP-18 silica gel and water as an eluent. The polarity of the eluent was then gradually decreased by the addition of acetone in the following steps: 5, 10, 20, 40, and 60 %. Fractions containing blue product were collected. For some compounds the last step of purification (RP-18 flash chromatography) had to be repeated two to three times to obtain pure product (≥ 95 % purity as determined by LC-MS, Table 1). The pooled product-containing fractions were evaporated under vacuum to remove the acetone and reduce water volume. The remaining water was subsequently removed by lyophilization to yield (up to 80 %) of the product as blue powder (Scheme 1 and Table 1).

General procedure B. Preparation of 4-substituted anthraquinone-2-sulfonate derivatives (68 and 69). To a 50 mL round bottom flask equipped with a magnetic stirring bar were 0.1 mmol of 1-aminoanthraquinone derivative (**12** or **27**) added, followed by 5 mL of 1 molar hydrochloric acid. The solution was cooled to 0–5 °C in an ice bath and a previously cooled solution of $NaNO_2$ (13.8 mg, 0.2 mmol, 2 equiv.) in 0.5 mL distilled water was dropwise added. After 5 min, the mixture was allowed to warm up to rt followed by addition of 30 mg of Zinc powder (1.0 mmol, 10 equiv.) and 5 mL ethanol. The resulting mixture was then allowed to stir at rt for ca. 30 second. The mixture was filtered off and the purple-colored filtrate was then purified by flash column chromatography on a reversed phase silica gel (RP-18) using a gradient of acetone in water (5 % and 20 %) as the eluent. Fractions containing the purple product were collected and evaporated in vacuum to remove acetone and decrease the volume of water to ca. 20 mL. Complete drying was achieved with a freeze dryer affording purple-colored products **66** and **67** in 36 % and 97 % yield, respectively (Scheme 3 and Table 1).

Sodium   1-amino-4-(2-chlorophenylamino)-9,10-dioxo-9,10-dihydroanthracene-2-sulfonate (14): Reaction conditions: according to general procedure A: Compound **6a** (81 mg, 0.2 mmol), 2-chloroaniline (51 mg, 0.4 mmol). MW conditions: 5 min, 120 °C, 100 W; pressure up to 10 bar. Analytical data: blue powder (36 % yield), mp > 300 °C. ^{1}H NMR (500 MHz): δ 7.20 (m, 1H, 4'-H), 7.42 (m, 2H, 5'-H, 6'-H), 7.61 (dd, 1H, 3'-H), 7.86 (m, 2H, 6-H, 7-H), 7.91 (s, 1H, 3-H), 8.27 (m, 2H, 5-H, 8-H), 10.00 (br, 2H, 1-NH$_2$), 11.95 (s, 1H, 4-NH). ^{13}C NMR (126 MHz): δ 109.61, 112.91, 122.79, 123.81, 125.48, 126.24, 126.50, 128.30, 130.48, 133.06, 133.56, 133.64, 134.32, 136.77, 139.32, 142.66, 144.70, 182.20, 183.47. LC-MS (m/z): 446 [M − Na$^+$ + NH$_4^+$]$^+$, 429 [M − Na$^+$ + H$^+$]$^+$, 427 [M − Na$^+$ + H$^+$]$^-$. Purity by HPLC-UV (254 nm)-ESI-MS: 99 %.

Sodium   1-amino-4-(2-methylphenylamino)-9,10-dioxo-9,10-dihydroanthracene-2-sulfonate (19): Reaction conditions: according to general procedures A: Compound **6a** (81 mg, 0.2 mmol), 2-methylaniline (43 mg, 0.4 mmol). MW conditions: 10 min, 120 °C, 100 W; pressure up to 10 bar. Yield 80 %. Purity by HPLC-UV (254 nm)-ESI-MS: 99 %.

Sodium   1-amino-4-(3-methylphenylamino)-9,10-dioxo-9,10-dihydroanthracene-2-sulfonate (20): Reaction conditions: according to general procedure A: Compound **6a** (81 mg, 0.2 mmol), 3-methylaniline (43 mg, 0.4 mmol). MW conditions: 10 min, 120 °C, 100 W; pressure up to 10 bar. Yield 70 %. Purity by HPLC-UV (254 nm)-ESI-MS: 99.1 %.

Sodium   1-amino-4-(4-methylphenylamino)-9,10-dioxo-9,10-dihydroanthracene-2-sulfonate (21): Reaction conditions: according to general procedure A: Compound **6a** (121.3 mg, 0.3 mmol), 4-methylaniline (64.3 mg, 0.6 mmol). MW conditions: 5 min, 120 °C, 100 W; pressure up to 10 bar. Yield 72 %. Purity by HPLC-UV (254 nm)-ESI-MS: 100 %.

Sodium 1-amino-4-(4-ethylphenylamino)-9,10-dioxo-9,10-dihydroanthracene-2-sulfonate

(24): Reaction conditions: according to general procedure A: Compound **6a** (81 mg, 0.2

mmol), 4-ethylaniline (48.5 mg, 0.4 mmol). MW conditions: 5 min, 120 °C, 100 W; pressure

up to 10 bar. Analytical data: blue powder (64 % yield), mp > 300 °C. ^{1}H NMR (500 MHz): δ

1.22 (t, 3H, 4'-CH$_2$*CH$_3$*), 2.64 (q, 2H, 4'-*CH$_2$*CH$_3$), 7.20 (d, 2H, 2'-H, 6'-H), 7.29 (d, 2H, 3'-H,

5'-H), 7.84 (m, 2H, 6-H, 7-H), 7.98 (s, 1H, 3-H), 8.27 (m, 2H, 5-H, 8-H), 10.10 (br, 2H, 1-

NH$_2$), 12.07 (s, 1H, 4-NH). ^{13}C NMR (126 MHz): δ 15.64, 27.75, 109.18, 111.03, 122.73,

123.61, 126.05, 126.15, 129.12, 132.85, 133.18, 133.76, 134.28, 136.81, 140.43, 141.59,

143.04, 144.39, 181.84, 182.30. LC-MS (m/z): 440 $[M - Na^+ + NH_4^+]^+$, 423 $[M - Na^+ + H^+]^+$,

421 $[M - Na^+ + H^+]^-$. Purity by HPLC-UV (254 nm)-ESI-MS: 99 %.

Sodium   1-amino-4-(3-propylphenylamino)-9,10-dioxo-9,10-dihydroanthracene-2-

sulfonate (25): Reaction conditions: according to general procedure A: Compound **6a** (121.3

mg, 0.3 mmol), 3-propylaniline (61 mg, 0.45 mmol). MW conditions: 15 min, 120 °C, 100

W; pressure up to 10 bar. Analytical data: blue powder (35 % yield), mp > 300 °C. ^{1}H NMR

(500 MHz): δ 0.91 (t, 3H, -CH$_2$CH$_2$*CH$_3$*), 1.63 (sext, 2H, -CH$_2$*CH$_2$*CH$_3$), 2.58 (t, 2H, -

*CH$_2$*CH$_2$CH$_3$), 7.03 (d, 1H, 6'-H), 7.10 (m, 2H, 2'-H, 4'-H), 7.35 (t, 1H, 5'-H), 7.85 (m, 2H, 6-

H, 7-H), 8.05 (s, 1H, 3-H), 8.28 (m, 2H, 5-H, 8-H), 12.07 (s, 1H, 4-NH). ^{13}C NMR (126

MHz): δ 13.65, 23.91 , 37.91, 109.06, 111.19, 120.32, 122.79, 123.02, 124.59, 125.90,

126.00, 129.41, 132.71, 133.09, 133.57, 134.12, 139.05, 140.93, 142.79, 143.94, 144.30,

181.72, 182.32. LC-MS (m/z): 454 $[M - Na^+ + NH_4^+]^+$, 437 $[M - Na^+ + H^+]^+$, 435 $[M - Na^+$

$+ H^+]^-$. Purity by HPLC-UV (220–700 nm)-ESI-MS: 97.7 %.

Sodium   1-amino-4-(2,3-dimethylphenylamino)-9,10-dioxo-9,10-dihydroanthracene-2-

sulfonate (33): Reaction conditions: according to general procedure A: Compound **6a** (81 mg,

0.2 mmol), 2,3-di-methylaniline (48.5 mg, 0.4 mmol). MW conditions: 5 min, 120 °C, 100 W;

pressure up to 10 bar. Yield 49 %. Purity by HPLC-UV (254 nm)-ESI-MS: 99 %.

Sodium 1-amino-4-(2,4-dimethylphenylamino)-9,10-dioxo-9,10-dihydroanthracene-2-sulfonate (34): Reaction conditions: according to general procedure A: Compound **6a** (81 mg, 0.2 mmol), 2,4-di-methylaniline (48.5 mg, 0.4 mmol). MW conditions: 5 min, 120 °C, 100 W; pressure up to 10 bar. Yield 60 %. Purity by HPLC-UV (254 nm)-ESI-MS: 99 %.

Sodium 1-amino-4-(2,5-dimethylphenylamino)-9,10-dioxo-9,10-dihydroanthracene-2-sulfonate (35): Reaction conditions: according to general procedure A: Compound **6a** (81 mg, 0.2 mmol), 2,5-di-methylaniline (48.5 mg, 0.4 mmol). MW conditions: 5 min, 120 °C, 100 W; pressure up to 10 bar. Yield 50 %. Purity by HPLC-UV (254 nm)-ESI-MS: 99.5 %.

Sodium 1-amino-4-(3,4-dimethoxyphenylamino)-9,10-dioxo-9,10-dihydroanthracene-2-sulfonate (37): Reaction conditions: According to general procedure A: Compound **6a** (121.3 mg, 0.3 mmol), 3,4-di-methoxyaniline (92 mg, 0.6 mmol). MW conditions: 5 min, 120 °C, 100 W; pressure up to 10 bar. Analytical data: blue powder (46 % yield), mp > 300 °C. ^{1}H NMR (500 MHz): δ 3.78 (s, 3H, -OCH$_3$), 3.80 (s, 3H, -OCH$_3$), 6.83 (dd, 1H, 6'-H, $J_{2',6'}$ 2.45 Hz, $J_{5',6'}$ 8.5 Hz), 6.94 (d, 1H, 2'-H, $J_{2',6'}$ 2.45 Hz), 7.03 (d, 1H, 5'-H, $J_{5',6'}$ 8.5 Hz), 7.85 (m, 2H, 6-H, 7-H), 7.98 (s, 1H, 3-H), 8.28 (m, 1H, 5-H, 8-H), 12.08 (s, 1H, 4-NH). ^{13}C NMR (126 MHz): δ 55.60, 55.74, 108.88, 110.34 (C-4a), 112.55, 115.94, 122.79, 125.82, 125.97, 131.96, 132.63, 132.90, 133.65, 134.12, 142.21, 142.91, 144.14, 146.42, 149.49, 181.57, 181.80. LCMS (m/z): 472 $[M - Na^+ + NH_4^+]^+$, 455 $[M - Na^+ + H^+]^+$, 453 $[M - Na^+ + H^+]^-$, Purity by HPLC-UV (220–700 nm)-ESI-MS: 98.5 %.

Sodium 1-amino-4-(3-methoxy-4-methylphenylamino)-9,10-dioxo-9,10-dihydroanthracene-2-sulfonate (39): Reaction conditions: According to general procedure A: Compound **6a** (121.3 mg, 0.3 mmol), 3-methoxy-4-methylaniline (82.3 mg, 0.6 mmol). MW conditions: 5 min, 120 °C, 100 W; pressure up to 10 bar. Analytical data: blue powder (44 % yield), mp > 300 °C. ^{1}H NMR (500 MHz): δ 2.17 (s, 1H, -CH$_3$), 3.81 (s, 3H, -OCH$_3$), 6.77 (dd, 1H, 6'-H, $J_{2',6'}$ 2.0 Hz, $J_{5',6'}$ 7.9 Hz), 6.89 (d, 1H, 2'-H, $J_{2',6'}$ 2.0 Hz), 7.19 (d, 1H, 5'-H,

$J_{5',6'}$ 7.9 Hz), 7.85 (m, 2H, 6-H, 7-H), 8.10 (s, 1H, 3-H), 8.28 (m, 1H, 5-H, 8-H), 12.10 (s, 1H, 4-NH). ^{13}C NMR (126 MHz): δ 15.69, 55.49, 106.40, 109.16, 111.05, 115.03, 122.20, 123.15, 126.03, 126.14, 131.08, 132.84, 133.18, 133.75, 134.28, 138.15, 141.46, 142.93, 144.40, 158.21, 181.83, 182.28. LCMS (m/z): 456 $[M - Na^+ + NH_4^+]^+$, 439 $[M - Na^+ + H^+]^+$, 437 $[M - Na^+ + H^+]^-$ Purity by HPLC-UV (220–700 nm)-ESI-MS: 98.3 %.

Sodium 1-amino-4-(4-chloro-2-methylamino)-9,10-dioxo-9,10-dihydroanthracene-2-sulfonate (40): Reaction conditions: according to general procedure A: Compound **6a** (81 mg, 0.2 mmol), 4-chloro-2-methylaniline (56.6 mg, 0.4 mmol). MW conditions: 24 min, 120 °C, 100 W; pressure up to 10 bar. Analytical data: blue powder (36 % yield), mp > 300 °C. ^{1}H NMR (500 MHz): δ 2.28 (s, 3H, 2'-CH$_3$), 7.27 (d, 1H, 6'-H, $J_{5',6'}$ 8.5 Hz), 7.33 (dd, 1H, 5'-H, $J_{3',5'}$ 2.4 Hz, $J_{5',6'}$ 8.5 Hz), 7.46 (d, 1H, 3'-H, $J_{3',5'}$ 2.4 Hz), 7.70 (s, 1H, 3-H), 7.84 (m, 2H, 6-H, 7-H), 8.26 (m, 2H, 5-H, 8-H), 10.05 (br, 2H, 1-NH$_2$), 11.88 (s, 1H, 4-NH). ^{13}C NMR (126 MHz): δ 17.69, 109.31, 111.46, 122.53, 125.89, 126.11, 126.20, 126.91, 129.03, 130.85, 132.92, 133.36, 133.67, 134.31, 134.70, 136.97, 131.40, 143.01, 144.36, 181.95, 182.83. LC-MS (m/z): 460 $[M - Na^+ + NH_4^+]^-$, 443 $[M - Na^+ + H^+]^+$, 441 $[M - Na^+ + H^+]^-$. Purity by HPLC-UV (254 nm)-ESI-MS: 99 %.

Sodium 1-amino-4-(4-chloro-3-methylphenylamino)-9,10-dioxo-9,10-dihydroanthracene-2-sulfonate (41): Reaction conditions: according to general procedure A: Compound **6a** (81 mg, 0.2 mmol), 4-chloro-3-methylaniline (56.6 mg, 0.4 mmol). MW conditions: 5 min, 120 °C, 100 W; pressure up to 10 bar. Analytical data: blue powder (40 % yield), mp > 300 °C. ^{1}H NMR (500 MHz): δ 2.34 (s, 3H, CH$_3$), 7.13 (dd, 1H, 6'-H, $J_{2',6'}$ 2.7 Hz, $J_{5',6'}$ 8.5 Hz), 7.27 (d, 1H, 2'-H, $J_{2',6'}$ 2.7 Hz), 7.44 (d, 1H, 5'-H, $J_{5',6'}$ 8.5 Hz),7.84 (m, 2H, 6-H, 7-H), 7.96 (s, 1H, 3-H), 8.25 (m, 2H, 5-H, 8-H), (br, 2H, 1-NH$_2$ not detectable), 11.90 (br, 1H, 4-NH). ^{13}C NMR (126 MHz): δ 19.80, 109.38, 111.96, 122.16, 122.86, 125.82, 126.09, 126.18, 128.69, 129.94, 132.96, 133.40, 133.63, 134.27, 137.02, 138.47, 140.48, 142.84, 144.52, 182.02, 182.82. LC-

MS (m/z): 460 [M − Na$^+$ + NH$_4^+$], 443 [M − Na$^+$ + H$^+$]$^+$, 441 [M − Na$^+$ + H$^+$]$^-$. Purity by HPLC-UV (254 nm)-ESI-MS: 99 %.

Sodium   1-amino-4-(4-hydroxy-3-methylphenylamino)-9,10-dioxo-9,10-dihydroanthracene-2-sulfonate (42): Reaction conditions: according to general procedure A: Compound **6a** (121.3 mg, 0.3 mmol), 4-amino-2-methylphenol (111 mg, 0.9 mmol)**.** MW conditions: 20 min, 100 °C, 100 W; pressure up to 10 bar. Analytical data: blue powder (40 % yield), mp > 300 °C. ^{1}H.NMR (500 MHz): δ 2.15 (s, 3H, CH$_3$) , 6.86 (d, 1H, 5'-H, $J_{5',6'}$ 8.4 Hz) , 6.93 (dd, 1H, 6'-H, $J_{5',6'}$ 8.4, $J_{2',6'}$ 2.6 Hz) , 7.01 (d, 1H, 2'-H, $J_{2',6'}$ 2.6 Hz) , 7.81 (s, 1H, 3-H) , 7.84 (m, 2H, 6-H, 7-H), 8.28 (m, 2H, 5-H, 8-H).^{13}C NMR (126 MHz): δ 15.94, 108.73, 109.68, 115.32, 122.57, 123.39, 125.23, 125.79, 125.94, 127.37, 129.58, 132.54, 132.73, 133.74, 134.11, 143.07, 143.28,143.97, 153.42, 181.41, 181.46. LC-MS (m/z): 425 [M − Na$^+$ + H$^+$]$^+$, 423 [M − Na$^+$ + H$^+$]$^-$.. Purity by HPLC-UV (254 nm)-ESI-MS: 96 %.

Sodium   1-amino-4-(4-fluoro-3-methoxyphenylamino)-9,10-dioxo-9,10-dihydroanthracene-2-sulfonate (43): Reaction conditions: According to general procedure A: Compound **6a** (121.3 mg, 0.3 mmol), 4-fuoro-3-methoxylaniline (84.7 mg, 0.6 mmol). MW conditions: 5 min, 120 °C, 100 W; pressure up to 10 bar. Analytical data: blue powder (43 % yield), mp > 300 °C . ^{1}H NMR (500 MHz): δ 3.86 (s, 3H, -OCH$_3$), 6.85 (m, 1H, 6'-H), 7.14 (dd, 1H, 2'-H, $^4J_{H-F}$ 7.8 Hz, $^4J_{2',6'}$ 2.5 Hz), 7.27 (dd, 1H, 5'-H, $^3J_{H-F}$ 11.35 Hz, $^4J_{5',6'}$ 8.6 Hz), 7.86 (m, 2H, 6-H, 7-H), 8.00 (s, 1H, 3-H), 8.28 (m, 1H, 5-H, 8-H), 11.96 (s, 1H, 4-NH). ^{13}C NMR (126 MHz): δ 56.52, 109.07, 109.79, 111.22, 115.36, 116.37, 122.72, 125.88, 126.01, 132.74, 133.14, 133.52, 134.12, 135.89, 141.06, 142.77, 144.26, 147.78, 149.65, 181.77, 182.40**.** LCMS (m/z): 460 [M − Na$^+$ + NH$_4^+$]$^+$, 443 [M − Na$^+$ + H$^+$]$^+$, 441 [M − Na$^+$ + H$^+$]$^-$ Purity by HPLC-UV (220–700 nm)-ESI-MS: 99.3 %.

Sodium 1-amino-4-(4-chloro-3-methoxyphenylamino)-9,10-dioxo-9,10-dihydroanthracene-2-sulfonate (44): Reaction conditions: According to general procedure A: Compound **6a** (121.3 mg, 0.3 mmol), 4-chloro-3-methoxylaniline (94.6 mg, 0.6 mmol)**.** MW conditions: 5 min, 120 °C, 100 W; pressure up to 10 bar. Analytical data: blue powder (40 % yield), mp > 300 °C. ^{1}H NMR (500 MHz): δ 3.88 (s, 3H, -OCH$_3$), 6.87 (dd, 1H, 6'-H, $J_{2',6'}$ 2.4 Hz, $J_{5',6'}$ 8.45 Hz), 7.10 (d, 1H, 2'-H, $J_{2',6'}$ 2.4 Hz), 7.44 (d, 1H, 5'-H, $J_{5',6'}$ 8.45 Hz), 7.86 (m, 2H, 6-H, 7-H), 8.10 (s, 1H, 3-H), 8.27 (m, 1H, 5-H, 8-H), 11.90 (s, 1H, 4-NH). ^{13}C NMR (126 MHz): δ 56.14, 107.60, 109.26, 112.08, 115.13, 116.00, 123.08, 125.92, 126.03, 130.31, 132.81, 133.28, 133.43, 134.10, 139.67, 139.80, 142.51, 144.43, 155.23, 181.88, 182.74. LC-MS (m/z):476 [M − Na$^+$ + NH$_4^+$]$^+$, 459 [M − Na$^+$ + H$^+$]$^+$, 457 [M − Na$^+$ + H$^+$]$^-$. Purity by HPLC-UV (220–700 nm)-ESI-MS: 99.7 %.

Sodium 1-amino-4 (2-carboxy-3-fluorophenylamino)-9,10-dioxo-9,10-dihydroanthracene-2-sulfonate (49): Reaction conditions: according to general procedure A: Compound **6a** (121.3 mg, 0.3 mmol), 2-amino-6-fluorobenzoic acid (93 mg, 0.6 mmol). MW conditions: 15 min, 120 °C, 100 W; pressure up to 10 bar. Analytical data: blue powder (40 % yield), mp > 300 °C. ^{1}H NMR (500 MHz): δ 6.78 (dd, 1H, 5'-H), 6.94 (d, 1H, 6'-H), 7.15 (dd, 1H, 4'-H), 7.82 (m, 2H, 6-H, 7-H), 8.10 (s,1H, 3-H)), 8.25 (m, 2H, 5-H, 8-H), 10.05 (br, 2H, 1-NH$_2$), 12.07 (s, 1H, 4-NH). ^{13}C NMR (126 MHz): δ 109.67, 110.09, 113.18, 116.83, 124.46, 126.27, 126.04, 127.18, 127.22 , 132.82, 133.13, 133.86, 134.22, 138.59, 139.03, 141.96, 144.59, 159.54, 166.02, 181.9, 182.2. (m/z): 474 [M − Na$^+$ + NH$_4^+$]$^+$, 455 [M − Na$^+$ + H$^+$]$^+$, 457 [M − Na$^+$ + H$^+$]$^-$. Purity by HPLC-UV (254 nm)-ESI-MS: 98 %.

Sodium 1-amino-4-(2-carboxy-4-hydroxyphenylamino)-9,10-dioxo-9,10-dihydroanthracene-2-sulfonate (52): Reaction conditions: according to general procedure A: Compound **6a** (81 mg, 0.2 mmol), 2-amino-5-hydroxybenzoic acid (61.3 mg, 0.4 mmol). MW conditions: 5 min, 120 °C, 100 W; pressure up to 10 bar. Analytical data: blue powder,

(68 % yield), mp > 300 °C. ^{1}H NMR (500 MHz): δ 7.00 (dd, 1H, 5'-H, $J_{3',5'}$ 2.9 Hz, $J_{5',6'}$ 8.7

Hz), 7.17 (d, 1H, 6'-H, $J_{5',6'}$ 8.7 Hz), 7.33 (d, 1H, 3'-H, $J_{3',5'}$ 2.9 Hz), 7.83 (m, 2H, 6-H, 7-H),

7.90 (s, 1H, 3-H), 8.24 (m, 2H, 5-H, 8-H), 9.7 (br, 2H, 1-NH$_2$), 12.27 (s, 1H, 4-NH). [13]C

NMR (126 MHz): δ 109.54, 112.69, 117.20, 120.36, 123.80, 124.19, 125.33, 126.03, 126.11,

132.04, 132.84, 133.09, 133.90, 134.24, 140.03, 142.17, 144.44, 153.4, 167.33, 181.88,

182.06. LC-MS (m/z): 555 [M – Na$^+$ + H$^+$]$^+$, 553 [M – Na$^+$ + H$^+$]$^-$. Purity by HPLC-UV (254

nm)-ESI-MS: 100 %.

Sodium 1-amino-4-(2-carboxy-4-nitrophenylamino)-9,10-dioxo-9,10-dihydroanthracene-

2-sulfonate (53): Reaction conditions: according to general procedure A: Compound **6a** (60.6

mg, 0.15 mmol), 2-amino-5-nitrobenzoic acid (246 mg, 1.35 mmol). MW conditions: 20 min,

110 °C, 100 W; pressure up to 10 bar. Analytical data: blue powder (21 % yield), mp > 300

°C. ^{1}H NMR (500 MHz): δ 7.10 (d, 1H, 6'-H, $J_{5',6'}$ 9.2 Hz) 7.86 (m, 2H, 6-H and 7-H) 8.09 (s,

1H, 3-H), 8.11 (dd, 1H, 5'-H, $J_{3',5'}$ 2.9 Hz, $J_{5',6'}$ 9.2 Hz) , 8.15 (m, 1H, 5-H or 8-H) , 8.24 (m,

1H, 5-H or 8-H), 8.77 (d, 1H, 3'-H, $J_{3',5'}$ 2.9 Hz). ^{13}C NMR (126 MHz): δ 111.28, 115.34,

121.37, 126.03, 126.10, 126.58, 128.03, 128.06, 130.95, 133.18, 133.42, 133.73, 133.92,

137.78, 139.84, 146.07, 149.67, 167.63, 182.93, 183.22. LC-MS (m/z): 501 [M – Na$^+$ +

NH$_4$$^+$]$^+$, 484 [M – Na$^+$ + H$^+$]$^+$, 482 [M– Na$^+$ + H$^+$]$^-$. Purity by HPLC-UV (254 nm)-ESI-MS:

95.7 %.

Sodium 1-amino-4-[4-(4-fluorophenylthio)phenylamino]-9,10-dioxo-9,10-

dihydroanthracene-2-sulfonate (58): Reaction conditions: according to general procedure

A: Compound **6a** (121.3 mg, 0.3 mmol), 4-(4-fluorophenylthio)aniline (131.5 mg, 0.6 mmol).

MW conditions: 15 min, 120 °C, 100 W; pressure up to 10 bar. Analytical data: blue powder

(41 % yield), mp > 300 °C. ^{1}H NMR (500 MHz): δ 7.06 (d, 2H, 3'-H, 5'-H), 7.13 (dd, 2H, 2"-

H, 6"-H), 7.24 (dd, 2H, 3"-H, 5"-H), 7.30 (d, 2H, 2'-H, 6'-H), 7.84 (m, 2H, 6-H, 7-H), 7.94

(s,1H, 3-H), 8.27 (m, 2H, 5-H, 8-H), 10.11 (br, 2H, 1-NH$_2$), 12.03 (s, 1H, 4-NH). ^{13}C NMR

(126 MHz): δ 109.2, 111.1, 116.6, 116.8, 119.4, 120.8, 120.9, 122.6, 125.5, 126.0, 126.1, 132.9, 133.2, 133.7, 134.0, 134.6, 141.6, 143.1, 144.4, 152.7, 154.3, 157.4, 159.4, 181.9, 182.4. LC-MS (m/z): 522 $[M - Na^+ + NH_4^+]^+$, 505 $[M - Na^+ + H^+]^+$, 503 $[M - Na^+ + H^+]^-$. Purity by HPLC-UV (254 nm)-ESI-MS: 99.5 %.

Sodium 1-amino-4-[4-(4-chlorophenylthio)phenylamino]-9,10-dioxo-9,10-dihydroanthracene-2-sulfonate (59): Reaction conditions: according to general procedure A: Compound **6a** (121.3 mg, 0.3 mmol), 4-(4-chlorophenylthio)aniline (141.4 mg, 0.6 mmol). MW conditions: 15 min, 120 °C, 100 W; pressure up to 10 bar. Analytical data: blue powder (25 % yield), mp > 300 °C. ^{1}H NMR (500 MHz): δ 7.10 (m, 4H, 3'-H, 5'-H, 2"-H, 6"-H), 7.32 (dd, 2H, 3"-H, 5"-H), 7.44 (d, 2H, 2'-H, 6'-H), 7.85 (m, 2H, 6-H, 7-H), 7.96 (s,1H, 3-H), 8.27 (m, 2H, 5-H, 8-H), 10.11 (br, 2H, 1-NH_2), 12.03 (s, 1H, 4-NH). ^{13}C NMR (126 MHz): δ 109.3, 111.3, 120.2, 120.4, 122.6, 125.4, 126.1, 126.2, 127.4, 130.1, 132.9, 133.3, 133.7, 134.3, 135.2, 141.4, 143.1, 144.4, 153.2, 155.9, 181.9, 182.5. LC-MS (m/z): 519 $[M - Na^+ + H^+]^-$. Purity by HPLC-UV (254 nm)-ESI-MS: 98.6 %.

Sodium 1-amino-4-[4-(4-bromophenylthio)phenylamino]-9,10-dioxo-9,10-dihydroanthracene-2-sulfonate (60): Reaction conditions: according to general procedure A: Compound **6a** (121.3 mg, 0.3 mmol), 4-(4-bromophenylthio)aniline (190 mg, 0.6 mmol). MW conditions: 15 min, 120 °C, 100 W; pressure up to 10 bar. Analytical data: blue powder (17 % yield), mp > 300 °C. ^{1}H NMR (500 MHz): δ 7.03 (d, 2H, 3'-H, 5'-H) 7.12 (d, 2H, 2"-H, 6"-H), 7.33 (dd, 2H, 3"-H, 5"-H), 7.56 (d, 2H, 2'-H, 6'-H), 7.85 (m, 2H, 6-H, 7-H), 7.96 (s,1H, 3-H), 8.27 (m, 2H, 5-H, 8-H), 10.10 (br, 2H, 1-NH_2), 12.03 (s, 1H, 4-NH). ^{13}C NMR (126 MHz): δ 109.3, 111.3, 115.2, 120.3, 120.7, 122.6, 125.3, 126.1, 126.2, 132.9, 133.0, 133.3, 135.3, 141.4, 144.4, 153.1, 156.5, 181.9, 182.5. LC-MS (m/z): 565 $[M - Na^+ + H^+]^+$, 563 $[M - Na^+ + H^+]^-$. Purity by HPLC-UV (254 nm)-ESI-MS: 96.1 %.

Sodium 1-amino-4-[4-(2,4-dimethylphenylthio)phenylamino]-9,10-dioxo-9,10-dihydroanthracene-2-sulfonate (61): Reaction conditions: according to general procedure A: Compound **6a** (121.3 mg, 0.3 mmol), 4-[(2,4-dimethylphenyl)thio]aniline (137.6 mg, 0.6 mmol). MW conditions: 15 min, 120 °C, 100 W; pressure up to 10 bar. Analytical data: blue powder (10 % yield), mp > 300 °C. ^{1}H NMR (500 MHz): δ 2.31, 2.28 (2s, 6H, 2CH$_3$), 7.04, 7.20 (m, 7H, 2'-H, 3'-H, 5'-H, 6'-H, 3''-H, 5''-H, 6''-H), 7.84 (m, 2H, 6-H, 7-H), 7.98 (s, 1H, 3-H), 8.25 (m, 2H, 5-H, 8-H), 10.05 (br, 2H, 1-NH$_2$), 11.95 (s, 1H, 4-NH). ^{13}C-NMR: δ 20.2, 20.7, 109.4, 112.0, 122.9, 123.7, 126.1, 126.2, 127.9, 129.5, 130.4, 130.9, 131.7, 132.9, 133.3, 133.6, 134.2, 138.1, 138.2, 139.5, 140.2, 142.8, 144.5, 182.0, 182.7. LC-MS (m/z): 531 [M − Na$^+$ + H$^+$]$^+$, 529 [M − Na$^+$ + H$^+$]$^-$. Purity by HPLC-UV (254 nm)-ESI-MS: 96.1 %.

Sodium 1-amino-4-[4-(2,5-dimethylphenylthio)phenylamino]-9,10-dioxo-9,10-dihydroanthracene-2-sulfonate (62): Reaction conditions: according to general procedure A: Compound **6a** (121.3 mg, 0.3 mmol), 4-[(2,5-dimethylphenyl)thio]aniline (137.6 mg, 0.6 mmol). MW conditions: 15 min, 120 °C, 100 W; pressure up to 10 bar. Analytical data: blue powder (7 % yield), mp > 300 °C. ^{1}H NMR (500 MHz): δ 2.23, 2.30 (2s, 6H, 2CH$_3$), 7.08, 7.23 (m, 7H, 2'-H, 3'-H, 5'-H, 6'-H, 3''-H, 4''-H, 6''-H), 7.84 (m, 2H, 6-H, 7-H), 8.00 (s, 1H, 3-H), 8.25 (m, 2H, 5-H, 8-H), 10.07 (br, 2H, 1-NH$_2$), 11.94 (s, 1H, 4-NH). ^{13}C-NMR: δ 19.8, 20.6, 109.4, 112.2, 123.0, 123.7, 126.1, 126.2, 128.9, 129.9, 130.7, 131.4, 132.6, 133.0, 133.2, 133.4, 133.6, 134.3, 135.9, 136.4, 138.6, 140.1, 142.8, 144.6, 182.0, 182.8. LC-MS (m/z): 531 [M − Na$^+$ + H$^+$]$^+$, 529 [M − Na$^+$ + H$^+$]$^-$. Purity by HPLC-UV (254 nm)-ESI-MS: 98.0 %.

Sodium 1-amino-4-[4-(3,4-dimethylphenylthio)phenylamino]-9,10-dioxo-9,10-dihydroanthracene-2-sulfonate (63): Reaction conditions: according to general procedure A: Compound **6a** (121.3 mg, 0.3 mmol), 4-[(3,4-dimethylphenyl)thio]aniline (137.6 mg, 0.6 mmol). MW conditions: 15 min, 120 °C, 100 W; pressure up to 10 bar. Analytical data: blue powder (7 % yield), mp > 300 °C. ^{1}H NMR (500 MHz): δ 2.21 (s, 6H, 2CH$_3$), 7.21 (m, 7H,

2'-H, 3'-H, 5'-H, 6'-H, 3''-H, 4''-H, 6''-H), 7.84 (m, 2H, 6-H, 7-H), 8.00 (s, 1H, 3-H), 8.25 (m, 2H, 5-H, 8-H), 10.06 (br, 2H, 1-NH$_2$), 11.93 (s, 1H, 4-NH). ^{13}C-NMR: δ 19.1, 19.4, 109.4, 112.1, 122.9, 123.6, 126.1, 126.2, 129.3, 130.8, 130.9, 131.1, 131.5, 132.7, 132.9, 133.4, 133.6, 134.2, 136.4, 137.9, 138.5, 140.1, 142.7, 144.6, 182.0, 182.8. LC-MS (m/z): 531 [M − Na$^+$ + H$^+$]$^+$, 529 [M − Na$^+$ + H$^+$]$^−$. Purity by HPLC-UV (254 nm)-ESI-MS: 95.6 %.

Sodium   1-amino-4-[4-(3-pyridin-3-ylmethylthio)phenylamino]-9,10-dioxo-9,10-dihydroanthra-cene-2-sulfonate (64): Reaction conditions: according to general procedure A: Compound **6a** (121.3 mg, 0.3 mmol), 4-[(pyridin-3-ylmethyl)thio]aniline (129.8 mg, 0.6 mmol). MW conditions: 15 min, 120 °C, 100 W; pressure up to 10 bar. Analytical data: blue powder (14 % yield), mp > 300 °C. ^{1}H NMR (500 MHz): δ 4.33 (s, 2H, CH$_2$), 7.21 (d, 2H, 2'-H, 6'-H), 7.39 (d, 2H, 3'-H, 5'-H), 7.64 (m, 1H, 5''-H), 7.84 (m, 2H, 6-H, 7-H), 7.97 (s, 1H, 3-H), 8.03 (s, 1H, 6''-H), 8.26 (m, 2H, 5-H, 8-H), 8.60 (2s, 2H, 2''-H, 4''-H), 11.89 (s, 1H, 4-NH). ^{13}C-NMR: δ 34.7, 109.4, 112.2, 123.0, 123.4, 125.2, 126.1, 126.2, 129.1, 132.6, 133.0, 133.4, 133.6, 134.3, 136.1, 138.7, 140.2, 140.8, 142.7, 144.6, 145.0, 146.2, 182.0, 182.8. LC-MS (m/z): 518 [M − Na$^+$ + H$^+$]$^+$, 516 [M − Na$^+$ + H$^+$]$^−$. Purity by HPLC-UV (254 nm)-ESI-MS: 98.6 %.

4-(3-Fluorophenylamino)-9,10-dioxo-9,10-dihydroanthracene-2-sulfonic   acid   (68): Reaction conditions: Compound **12** (41 mg, 0.1 mmol) was reacted according to general procedure C. Analytical data: reddish purple powder (97 % yield), mp > 300 °C. ^{1}H NMR (600 MHz): δ 7.07 (td, 1H, 6'-H), 7.23 (m, 2H, 2'-H, 5'-H), 7.51 (m, 1H, 4'-H), 7.80 (d, 1H, 1-H or 3-H , $J_{1,3}$ 1.47 Hz), 7.86 (d, 1H, 1-H or 3-H , $J_{1,3}$ 1.47 Hz), 7.90 (td, 1H, 6-H or 7-H), 7.94 (td, 1H, 6-H or 7-H), 8.20 (dd, 1H, 5-H or 8-H), 8.25 (dd, 1H, 5-H or 8-H), 11.21 (s, 1H, 4-NH).^{13}C NMR (151 MHz) δ 39.52, 110.16, 110.32, 111.46, 111.60, 113.94, 115.53, 116.05, 119.18, 119.20, 126.51, 126.66, 131.26, 131.33, 132.49, 133.98, 134.17, 134.30, 134.68,

140.94, 141.01, 147.72, 154.35, 161.98, 163.60, 182.30, 184.50. LC-MS (m/z): 415 [M – H^+ + NH_4^+]$^+$, 398 [M]$^+$, 396 [M]$^-$. Purity by HPLC-UV (220–650 nm)-ESI-MS: 98.5 %.

4-(3-Methoxyphenylamino)-9,10-dioxo-9,10-dihydroanthracene-2-sulfonic acid (69): Reaction conditions: Compound **27** (42 mg, 0.1 mmol) was reacted according to general procedure C. Analytical data: reddish purple powder (38 % yield), mp > 300 °C. ^{1}H NMR (500 MHz) δ 3.80 (s, 1H, -OCH$_3$), 6.84 (m, 1H, 6'-H), 6.94 (m, 2H, 2'-H, 4'-H), 7.39 (m, 1H, 5'-H), 7.81 (d, 1H, 1-H or 3-H , $J_{1,3}$ 1.5 Hz), 7.83 (d, 1H, 1-H or 3-H , $J_{1,3}$ 1.5 Hz), 7.90 (td, 1H, 6-H or 7-H), 7.95 (td, 1H, 6-H or 7-H), 8.20 (dd, 1H, 5-H or 8-H), 8.27 (dd, 1H, 5-H or 8-H), 11.24 (s, 1H, 4-NH). ^{13}C NMR (126 MHz) δ 55.20, 109.27, 110.86, 113.28, 115.08, 115.70, 116.14, 126.46, 126.61, 130.47, 132.51, 133.84, 134.15, 134.25, 134.61, 140.03, 148.47, 154.31, 160.36, 182.35, 184.35. LC-MS (m/z): 427 [M – H^+ + NH_4^+]$^+$, 410 [M]$^+$, 408 [M]$^-$. Purity by HPLC-UV (220–600 nm)-ESI-MS: 95.2 %.

Retroviral transfection of 1321N1 astrocytoma cells with human P2Y$_1$, P2Y$_4$, and P2Y$_6$ receptors. Transfection of 1321N1 astrocytoma cells with human P2Y$_1$, P2Y$_4$, and P2Y$_6$ receptors was performed as previously described.[59] Transfection with the human P2Y$_2$ receptor was done in analogy (see Supporting Information). Briefly, the coding sequence of the respective receptor was cloned into the pQCXIN or pLXSN retroviral vector, amplified, purified, and sequenced prior to the transfection of GP$^+$env AM-12 packaging cells together with vesicular stomatitis virus G (VSV-G) protein DNA using lipofectamine 2000. After 16 h, 3 ml of Dulbecco's modified Eagle's medium (DMEM) containing 10 % fetal calf serum, 1 % of a penicillin/streptomycin solution (final concentrations: penicillin = 100 U/ml, streptomycin = 0.1 mg/ml), and sodium butyrate (5 mM) was given to the packaging cells and these were kept at 32 °C and 5 % CO_2 for 48 h during which the viral vectors containing the

receptor sequence were produced and released into the surrounding medium. These were harvested, filtered (45 µm filter pore diameter) and given to 1321N1 astrocytoma cells that do not intrinsically express P2 receptors at a detectable level. Polybrene solution (6 µl, 4 mg/ml in H_2O, filtered) was added. After 2.5 hours, the virus-containing medium was discarded and DMEM supplemented with 10 % fetal calf serum and 1 % of a penicillin/streptomycin solution (final concentrations: penicillin = 100 U/ml, streptomycin = 0.1 mg/ml) was given to the cells. These were incubated for two days, followed by selection of successfully transfected cells with geneticin resistance by adding G418 (200 µg/ml) to the medium. Single cells were selected and grown into monoclonal colonies in case of the $P2Y_2$ and $P2Y_4$ receptor expressing cells.

Pharmacological evaluation of the compounds at human $P2Y_1$, $P2Y_2$, $P2Y_4$, and $P2Y_6$ receptors. All experiments were performed using 1321N1 human astrocytoma cells stably expressing the respective human P2Y receptor subtype. The cells were grown in T175 tissue culture flasks (175 cm^2 area) containing 25-30 mL DMEM supplemented with 10 % fetal calf serum, 200 µg/mL G418, and 1 % of a penicillin/streptomycin solution (final concentrations: penicillin = 100 U/mL, streptomycin = 0.1 mg/mL). DMEM and supplements were purchased from Invitrogen (Life Technologies GmbH, Darmstadt, Germany). The flasks were kept at 37 °C in a humidified atmosphere (96 % relative humidity) containing 5 % CO_2. Cells were maintained in the exponential growth phase throughout and regularly tested for mycoplasma contamination.

Calcium-mobilization assays. Calcium measurements were performed as previously described.[60] Briefly, 1321N1 human astrocytoma cells stably transfected with the coding sequence for the respective human P2Y receptor were used. Approximately 24 h prior to

testing, the nutrient medium was discarded and the cells rinsed with phosphate-buffered saline before detachment using 0.05 % trypsin / 0.6 mM EDTA. The cells were then suspended in DMEM with the supplements described above and dispensed into sterile, black, flat, clear bottom 96-well polystyrene microplates with lid (Corning® 3340) at 50,000 cells per well. The microplates were incubated at 37 °C in humidified air with 5 % CO_2, during which the cells adhered to the coated bottom of the wells. Test compounds were investigated by measuring their inhibition of $P2Y_1$, $P2Y_2$, $P2Y_4$, or $P2Y_6$ receptor-mediated intracellular calcium mobilization using a FlexStation 3® (Molecular Devices GmbH, Biberach an der Riss, Germany) plate reader. At the start of the assay, the plated cells were loaded with fluo-4 acetoxymethyl ester (Life Technologies GmbH, Darmstadt, Germany) for 1 h. Excess dye was subsequently removed and Hank's balanced salt solution (HBSS) buffer given to the cells. Afterwards, the cells were pre-incubated with the test compound for 30 min. Using the pipetting function of the microplate reader, the physiological ligand was injected at a concentration that corresponds to its EC_{80}: 500 nM ADP for the $P2Y_1$, 500 nM UTP for the $P2Y_2$ and $P2Y_4$, 750 nM UDP for the $P2Y_6$ receptor. The final volume was 200 µl per well. Fluorescence was measured at 525 nm following excitation at 488 nm. At least three independent experiments were performed in duplicates. IC_{50} values were calculated by non-linear regression using Prism® 5.0 (GraphPad Software, San Diego, CA, USA).

Homology modeling of the human $P2Y_4$ receptor. A homology model of the human $P2Y_4$ receptor was created based on the X-ray co-crystal structure of the human $P2Y_1$ receptor with the nucleotide-derived antagonist MRS2500 (PDB ID: 4XNW.pdb, resolution: 2.7 Å).[56] The structure was downloaded from the RSCB (Research Collaboratory for Structural Bioinformatics) Protein Data Bank (http://www.rcsb.org/) and used as a template for generating the homology model of the human $P2Y_4$ receptor.[61] The amino acid sequence of the human $P2Y_4$ receptor with the accession number P51582 was retrieved from UniProtKB

sequence database.[62] The sequences of the human $P2Y_1$ and $P2Y_4$ receptors were aligned using Clustal Omega and AlignMe (Supplementary Figure 58).[63,64] The resulting alignments were manually adjusted for improving the alignment, particularly in the transmembrane and extracellular loop region 2 (ECL2). An overall sequence identity of 41.8 % and a similarity of 60.2 % between the human $P2Y_1$ and $P2Y_4$ receptors was calculated. The resulting alignment was used as input for generating homology models of the human $P2Y_4$ receptor using Modeller9.16.[65,66] From the 750 models generated, the best model was selected on the basis of the Discrete Optimized Protein Energy (DOPE) score included in Modeller, manual visualization of the presence of an ionic lock between Asp187 and Arg29, and analysis of the binding sites. The overall structural quality was confirmed by a Ramachandran Plot (Supplementary Figure 59),[67] and sequence-structure compatibility of the model was ensured using PROSA II profile analysis (Supplementary Figure 60).[68] Possible binding sites were identified using the SiteFinder module from Molecular Operating Environment (MOE 2014.09).[69]

Docking studies. Docking simulations were performed using Induced Fit Docking (IFD) and Glide as implemented in Schrödinger release 2016.[70–72] Prior to docking, the homology model of the human $P2Y_4$ receptor was prepared using the Protein Preparation Wizard at pH 7.4 and with forcefield Optimized Potentials for Liquid Simulations Version 3 (OPLS3) implemented in Schrödinger. The ligands were prepared using the implemented LigPrep module and the OLPS3 force field in possible states at pH 7.4 ± 1.0. The conformations of the docked ligands within an energy window of 2.5 kcal/mol were considered. For Glide docking, the following standard parameters were selected: receptor van der Waals scaling: 0.50; ligand van der Waals scaling: 0.50, and a maximum of 20 poses per ligand. Residues within 5.0 Å of the ligand poses were refined and the side chains were optimized. The best docking pose was selected based on the IFD score and Prime Energy values. The compounds were subsequently

docked to the best scoring complex obtained for compound **61**. A receptor grid center was

specified on the basis of the transformed position of the allosteric antagonist MRS2500 from

the human $P2Y_1$ receptor structure, with a cubic grid side length of 10 Å. As precision setting,

XP (extra precision) was chosen. Following Glide docking, the resulting poses were selected

using the IFD scores and Prime Energy as representative values.

Supporting Information Available: LC-MS spectra of RB-2 P (**2'**); ^{1}H NMR, ^{13}C NMR,

and DEPT 135 NMR spectra of the newly synthesized anthraquinone derivatives; description

of the β-arrestin recruitment assay used for measuring $P2Y_{12}$ receptor antagonism; multiple

sequence alignment of P2Y receptor subtypes.

Abbreviations.

2MeSADP, 2-Methylthioadenosine-5'-diphosphate;

APP   Amyloid precursor protein

DMEM   Dulbecco's modified Eagle's medium

ECL   Extracellular loop

GIT   Gastrointestinal tract

IFD   Induced fit docking

MRS2500   2-Iodo-N^6-methyl-(N)-methanocarba-2'-deoxyadenosine-3',5'-bisphosphate

PPADS   Pyridoxalphosphate-6-azophenyl-2',4'-disulfonic acid

RB-2   Reactive Blue 2

SEM   Standard error of the mean

TM   Transmembrane region

UTP   Uridine-5'-triphosphate

Author Information.

*Corresponding authors:

Dr. Christa E. Müller

Pharmazeutisches Institut

Pharmazeutische Chemie I

An der Immenburg 4, D-53121 Bonn, Germany

Phone: +49-228-73-2301

Fax: +49-228-73-2567

christa.mueller@uni-bonn.de

Dr. Younis Baqi

Department of Chemistry

Faculty of Science, Sultan Qaboos University

PO Box 36, Postal Code 123, Muscat, Oman

Phone: +968-24141473

Fax: +968-24141469

baqi@squ.edu.om

Notes:

The authors declare no competing financial interest.

References

(1)   Jacobson, K. A.; Müller, C. E. Medicinal chemistry of adenosine, P2Y and P2X receptors. *Neuropharmacology* **2016,** *104*, 31–49.

(2)   King, B. F.; Burnstock, G. Purinergic receptors. In *Understanding G Protein-coupled Receptors and their Role in the CNS*; Pangalos, M.; Davies, C., Eds.; Oxford University Press, 2002; pp. 422–438.

(3)   Burnstock, G. Introduction: P2 receptors. *Curr. Top. Med. Chem.* **2004**, *4*, 793–803.

(4)   Jacobson, K.; Jarvis, M. F.; Williams, M. Purine and pyrimidine (P2) receptors as drug targets. *J. Med. Chem.* **2002**, *45*, 4057–4093.

(5)   Savi, P.; Herbert, J. M. Clopidogrel and ticlopidine: $P2Y_{12}$ adenosine diphosphate-receptor antagonists for the prevention of atherothrombosis. *Semin. Thromb. Hemostasis* **2005**, *31*, 174–183.

(6)   Angiolillo, D. J.; Luis Ferreiro, J. Platelet adenosine diphosphate $P2Y_{12}$ receptor antagonism: benefits and limitations of current treatment strategies and future directions. *Rev. Esp. Cardiol.* **2010**, *63*, 60–76.

(7)   Teng, R.; Oliver, S.; Hayes, M.; Butler, K. Absorption, distribution, metabolism, and excretion of ticagrelor in healthy subjects. *Drug Metab. Dispos.* **2010**, *38*, 1514–1521.

(8)   Kim, C.-H.; Kim, H.-Y.; Lee, H. S.; Chang, S. O.; Oh, S.-H.; Lee, J. H. $P2Y_4$-mediated regulation of Na^+ absorption in the reissner's membrane of the cochlea. *J. Neurosci.* **2010**, *30*, 3762–3769.

(9)   Marcus, D. C.; Liu, J.; Lee, J. H.; Scherer, E. Q.; Scofield, M. A.; Wangemann, P.

Apical membrane P2Y$_4$ purinergic receptor controls K$^+$ secretion by strial marginal cell epithelium. *Cell Commun. Signaling* **2005**, *3*, 13.

(10) Burrell, H. E.; Bowler, W. B.; Gallagher, J. A.; Sharpe, G. R. Human keratinocytes express multiple P2Y-receptors: evidence for functional P2Y$_1$, P2Y$_2$, and P2Y$_4$ receptors. *J. Invest. Dermatol.* **2003**, *120*, 440–447.

(11) Song, X.; Guo, W.; Yu, Q.; Liu, X.; Xiang, Z.; He, C.; Burnstock, G. Regional expression of P2Y$_4$ receptors in the rat central nervous system. *Purinergic Signalling* **2011**, *7*, 469–488.

(12) Communi, D.; Pirotton, S.; Parmentier, M.; Boeynaems, J. Cloning and functional expression of a human uridine nucleotide receptor. *J. Biol. Chem.* **1995**, *270*, 30849–30852.

(13) Robaye, B.; Ghanem, E.; Wilkin, F.; Fokan, D.; Van Driessche, W.; Schurmans, S.; Boeynaems, J.-M.; Beauwens, R. Loss of nucleotide regulation of epithelial chloride transport in the jejunum of p2y4 -null mice. *Mol. Pharmacol.* **2003**, *63*, 777–783.

(14) Kunzelmann, K.; Mall, M. Electrolyte transport in the mammalian colon : mechanisms and implications for disease. *Physiol. Rev.* **2002**, *82*, 245–289.

(15) Ghanem, E.; Robaye, B.; Leal, T.; Leipziger, J.; Van Driessche, W.; Beauwens, R.; Boeynaems, J.-M. The role of epithelial P2Y$_2$ and P2Y$_4$ receptors in the regulation of intestinal chloride secretion. *Br. J. Pharmacol.* **2005**, *146*, 364–369.

(16) DuBose, D. R.; Wolff, S. C.; Qi, A.-D.; Naruszewicz, I.; Nicholas, R. A. Apical targeting of the P2Y$_4$ receptor is directed by hydrophobic and basic residues in the cytoplasmic tail. *Am. J. Physiol. Cell Physiol.* **2013**, *304*, C228–C239.

(17) Tran, M. D. P2 receptor stimulation induces amyloid precursor protein production and

secretion in rat cortical astrocytes. *Neurosci. Lett.* **2011**, *492*, 155–159.

(18) Horckmans, M.; Robaye, B.; Léon-Gómez, E.; Lantz, N.; Unger, P.; Dol-Gleizes, F.; Clouet, S.; Cammarata, D.; Schaeffer, P.; Savi, P.; Gachet, C.; Balligand, J.-L.; Dessy, C.; Boeynaems, J.-M.; Communi, D. P2Y$_4$ nucleotide receptor: a novel actor in post-natal cardiac development. *Angiogenesis* **2012**, *15*, 349–360.

(19) Brunschweiger, A.; Müller, C. E. P2 receptors activated by uracil nucleotides - an update. *Curr. Med. Chem.* **2006**, *24*, 289–312.

(20) Gachet, C. Regulation of platelet functions by P2 receptors. *Annu. Rev. Pharmacol. Toxicol.* **2006**, *46*, 277–300.

(21) Schwiebert, E. M.; Zsembery, A.; Geibel, J. P. Cellular mechanisms and physiology of nucleotide and nucleoside release from cells: current knowledge, novel assays to detect purinergic agonists, and future directions. In *Extracellular Nucleotides and Nucleosides: Release, Receptors, and Physiological & Pathophysiological Effects*; Schwiebert, E. M., Ed.; Academic press. Elsevier Science (USA), 2003; p. 76.

(22) Bogdanov, Y. D.; Wildman, S. S.; Clements, M. P.; King, B. F.; Burnstock, G. Molecular cloning and characterization of rat P2Y$_4$ nucleotide receptor. *Br. J. Pharmacol.* **1998**, *124*, 428–430.

(23) Wildman, S. S.; Unwin, R. J.; King, B. F. Extended pharmacological profiles of rat P2Y$_2$ and rat P2Y$_4$ receptors and their sensitivity to extracellular H$^+$ and Zn^{2+} ions *Br. J. Pharmacol.* **2003**, *140*, 1177–1186.

(24) Baqi, Y.; Lee, S.-Y.; Iqbal, J.; Ripphausen, P.; Lehr, A.; Scheiff, A. B.; Zimmermann, H.; Bajorath, J.; Müller, C. E. Development of potent and selective inhibitors of ecto-5'-nucleotidase based on an anthraquinone scaffold. *J. Med. Chem.* **2010**, *53*, 2076–

2086.

(25) Malik, E. M.; Müller, C. E. Anthraquinones as pharmacological tools and drugs. *Med. Res. Rev.* **2016**, *36*, 705–748.

(26) Baqi, Y. Anthraquinones as a privileged scaffold in drug discovery targeting nucleotide-binding proteins. *Drug Discovery Today* **2016**, *21*, 1571–1577.

(27) Baqi, Y.; Müller, C. E. Rapid and efficient microwave-assisted copper (0)-catalyzed ullmann coupling reaction: general access to anilinoanthraquinone derivatives. *Org. Lett.* **2007**, *9*, 1271–1274.

(28) Baqi, Y.; Müller, C. E. Synthesis of alkyl- and aryl-amino-substituted anthraquinone derivatives by microwave-assisted copper(0)-catalyzed ullmann coupling reactions. *Nat. Protoc.* **2010**, *5*, 945–953.

(29) Weyler, S.; Baqi, Y.; Hillmann, P.; Kaulich, M.; Hunder, A. M.; Müller, I. A.; Müller, C. E. Combinatorial synthesis of anilinoanthraquinone derivatives and evaluation as non-nucleotide-derived P2Y$_2$ receptor antagonists. *Bioorg. Med. Chem. Lett.* **2008**, *18*, 223–227.

(30) Baqi, Y.; Atzler, K.; Köse, M.; Glänzel, M.; Müller, C. E. High-affinity , non-nucleotide-derived competitive antagonists of platelet P2Y$_{12}$ receptors. *J. Med. Chem.* **2009**, *52*, 3784–3793.

(31) Baqi, Y.; Hausmann, R.; Rosefort, C.; Rettinger, J.; Schmalzing, G.; Müller, C. E. Discovery of potent competitive antagonists and positive modulators of the P2X2 receptor. *J. Med. Chem.* **2011**, *54*, 817–830.

(32) Baqi, Y.; Müller, C. E. Convergent synthesis of the potent P2Y receptor antagonist MG 50-3-1 based on a regioselective ullmann coupling reaction. *Molecules* **2012**, *17*,

2599–2615.

(33)   Baqi, Y.; Weyler, S.; Iqbal, J.; Zimmermann, H.; Müller, C. E. Structure-activity relationships of anthraquinone derivatives derived from bromaminic acid as inhibitors of ectonucleoside triphosphate diphosphohydrolases (E-NTPDases). *Purinergic Signalling* **2009**, *5*, 91–106.

(34)   Baqi, Y. Ecto-nucleotidase inhibitors : recent developments in drug discovery. *Mini-Rev. Med. Chem.* **2015**, *15*, 21–33.

(35)   Malik, E. M.; Baqi, Y.; Müller, C. E. Syntheses of 2-substituted 1-amino-4-bromoanthraquinones (bromaminic acid analogues) – precursors for dyes and drugs. *Beilstein J. Org. Chem.* **2015**, *11*, 2326–2333.

(36)   Malik, E. M.; Rashed, M.; Wingen, L.; Baqi, Y.; Müller, C. E. Ullmann reactions of 1-amino-4-bromoanthraquinones bearing various 2-substituents furnishing novel dyes. *Dyes Pigm.* **2016**, *131*, 33–40.

(37)   Hoffmann, K.; Baqi, Y.; Morena, M. S.; Glänzel, M.; Müller, C. E.; Kügelgen, I. Von. Interaction of new , very potent non-nucleotide antagonists with arg256 of the human platelet P2Y$_{12}$ receptor. *J. Pharmacol. Exp. Ther.* **2009**, *331*, 648–655.

(38)   Baqi, Y.; Hausmann, R.; Rosefort, C.; Rettinger, J.; Schmalzing, G.; Müller, C. E. Discovery of potent competitive antagonists and positive modulators of the P2X2 receptor. *J. Med. Chem.* **2011**, *54*, 817–830.

(39)   Baqi, Y.; Müller, C. E. Efficient and mild deamination procedure for 1-aminoanthraquinones yielding a diverse library of novel derivatives with potential biological activity. *Tetrahedron Lett.* **2012**, *53*, 6739–6742.

(40)   Fiene, A.; Baqi, Y.; Malik, E. M.; Newton, P.; Li, W.; Lee, S.; Hartland, Elizabeth L.

Müller, C. E. Inhibitors for the bacterial ectonucleotidase lp1ntpdase from legionella pneumophila. *Bioorg. Med. Chem*. **2016**, *24*, 4363–4371.

(41)   Glänzel, M.; Bültmann, R.; Starke, K.; Frahm, A. W. Constitutional isomers of reactive blue 2 – selective P2Y-receptor antagonists? *Eur. J. Med. Chem.* **2003**, *38*, 303–312.

(42)   Glänzel, M.; Bültmann, R.; Starke, K.; Frahm, A. W. Structure-activity relationships of novel P2-receptor antagonists structurally related to reactive blue 2. *Eur. J. Med. Chem*. **2005**, *40*, 1262–1276.

(43)   Burton, S. J.; McLoughlin, S. B.; Stead, C. V.; Lowe, C. R. Design and applications of biomimetic anthraquinone dyes 1. synthesis and characterization of terminal ring isomers of c.i. reactive blue 2. *J. Chromatogr. A* **1988**, *435*, 127–137.

(44)   Müller, C.E.; Schiedel, A.C.; Baqi, Y. Allosteric modulators of rhodopsin-like G protein-coupled receptors: opportunities in drug development. *Pharmacol. Ther*. **2012**, *135*, 292–315.

(45)   Böhme, H.-J.; Kopperschläger, G.; Schulz, J.; Hofmann, E. Affinity chromatography of phosphofructokinase using cibacron blue F3G-A. *J. Chromatogr. A* **1972**, *69*, 209–214.

(46)   Bornmann, L.; Hess, B. Interaction of cibacron dyes with dehydrogenases and kinases. *Z. Naturforsch.* **1977**, *32c*, 756–759.

(47)   Ashton, A. R.; Polya, G. M. The specific interaction of cibacron and related dyes with cyclic nucleotide phosphodiesterase and lactate dehydrogenase. *Biochem. J.* **1978**, *175*, 501–506.

(48)   Beissner, R. S.; Rudolph, F. B. Interaction of cibacron blue 3G-A and related dyes

with nucleotide-requiring enzymes. *Arch. Biochem. Biophys.* **1978**, *189*, 76–80.

(49)　Prestera, T.; Prochaska, H. J.; Talalay, P. Inhibition of NAD(P)H:(quinone-acceptor) oxidoreductase by cibacron blue and related anthraquinone dyes: a structure-activity study. *Biochemistry* **1992**, *31*, 824–833.

(50)　Biellmann, J.; Samama, J.; Branden, C. I.; Eklund, H. X-ray studies of the binding of cibacron blue F3GA to liver alcohol dehydrogenase. *Eur. J. Biochem.* **1979**, *102*, 107–110.

(51)　Monaghan, C.; Holland, S.; Dale, J. W. The interaction of anthraquinone dyes with the plasmid-mediated oxa-2 beta-lactamase. *Biochem. J.* **1982**, *205*, 413–417.

(52)　Liu, Y. C.; Ledger, R.; Stellwagen, E. Quantitative analysis of protein: immobilized dye interaction. *J. Biol. Chem.* **1984**, *259*, 3796–3799.

(53)　Roy, S.; Large, R. J.; Akande, A. M.; Kshatri, A.; Webb, T. I.; Domene, C.; Sergeant, G. P.; McHale, N. G.; Thornbury, K. D.; Hollywood, M. A. Development of GoSlo-SR-5-69, a potent activator of large conductance Ca^{2+}-activated K^+ (BK) channels. *Eur. J. Med. Chem.* **2014**, *75*, 426–437.

(54)　Zhang, K.; Zhang, J.; Gao, Z.G.; Zhang, D.; Zhu, L.; Han, G.W.; Moss, S.M.; Paoletta, S.; Kiselev, E.; Lu, W.; Fenalti, G.; Zhang, W.; Müller, C.E.; Yang, H.; Jiang, H.; Cherezov, V.; Katritch, V.; Jacobson, K.A.; Stevens, R.C.; Wu, B.; Zhao, Q. Structure of the human $P2Y_{12}$ receptor in complex with an antithrombotic drug. *Nature* **2014**, *509*, 115–118.

(55)　Zhang, J.; Zhang, K.; Gao, Z.G.; Paoletta, S.; Zhang, D.; Han, G.W.; Li, T.; Ma, L.; Zhang, W.; Müller, C.E.; Yang, H.; Jiang, H.; Cherezov, V.; Katritch, V.; Jacobson, K.A.; Stevens, R.C.; Wu, B.; Zhao, Q. Agonist-bound structure of the human $P2Y_{12}$
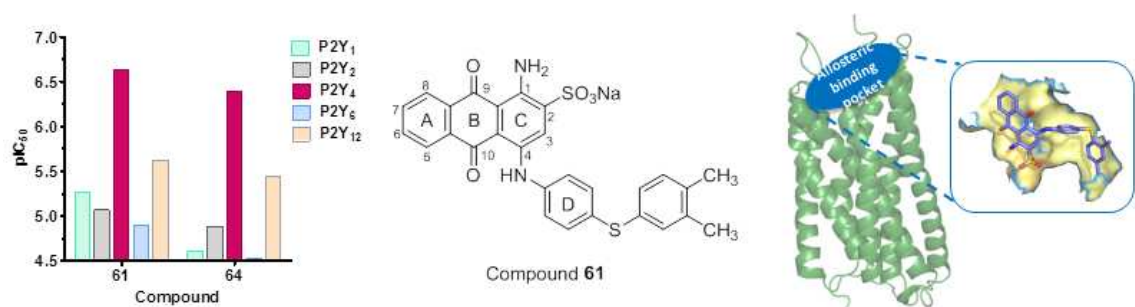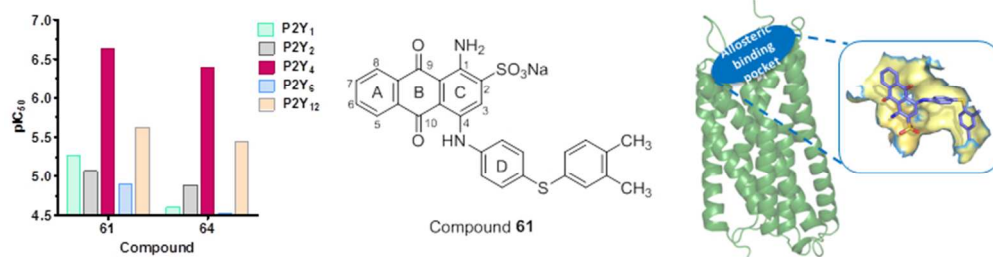
receptor. *Nature* **2014**, *509*, 119–122.

(56) Zhang, D.; Gao, Z.G.; Zhang, K.; Kiselev, E.; Crane, S.; Wang, J.; Paoletta, S.; Yi, C.; Ma, L.; Zhang, W.; Han, G.W.; Liu, H.; Cherezov, V.; Katritch, V.; Jiang, H.; Stevens, R.C.; Jacobson, K.A.; Zhao, Q.; Wu, B. Two disparate ligand-binding sites in the human P2Y$_1$ receptor. *Nature* **2015**, *520*, 317–321.

(57) Yuan, S.; Chan, H.C.; Vogel, H.; Filipek, S.; Stevens, R.C.; Palczewski, K. The molecular mechanism of P2Y1 receptor activation. *Angew. Chem. Int. Ed. Engl*. **2016**, *55*, 10331–10335.

(58) Rasmussen, C. R.; Gardocki, J. F.; Plampin, J. N.; Twardzik, B. L.; Reynolds, B. E.; Molinari, a J.; Schwartz, N.; Bennetts, W. W.; Price, B. E.; Marakowski, J. 2-Pyrrolidinylideneureas, a new class of central nervous system agents. *J. Med. Chem.* **1978**, *21*, 1044–1054.

(59) Hillmann, P.; Ko, G. Y.; Spinrath, A.; Raulf, A.; von Kügelgen, I.; Wolff, S. C.; Nicholas, R. A.; Kostenis, E.; Höltje, H. D.; Müller, C. E. Key determinants of nucleotide-activated G protein-coupled P2Y$_2$ receptor function revealed by chemical and pharmacological experiments , mutagenesis and homology modeling. *J. Med. Chem*. **2009**, *52*, 2762–2775.

(60) Hernandez-Olmos, V.; Abdelrahman, A.; El-Tayeb, A.; Freudendahl, D.; Weinhausen, S.; Müller, C. E. N-substituted phenoxazine and acridone derivatives: structure-activity relationships of potent P2X4 receptor antagonists. *J. Med. Chem.* **2012**, *55*, 9576–9588.

(61) Berman, H. M.; Westbrook, J.; Feng, Z.; Gilliland, G.; Bhat, T. N.; Weissig, H.; Shindyalov, I. N.; Bourne, P. E. The Protein Data Bank. *Nucleic Acids Res.* **2000**, *28*,

235–242.

(62) The UniProt Consortium, UniProt: a hub for protein information. *Nucleic Acids Res.* **2015**, *43* (Database issue), D204–D212.

(63) Sievers, F.; Wilm, A.; Dineen, D.; Gibson, T. J.; Karplus, K.; Li, W.; Lopez, R.; McWilliam, H.; Remmert, M.; Söding, J.; Thompson, J. D.; Higgins, D. G. Fast, scalable generation of high-quality protein multiple sequence alignments using Clustal Omega *Mol. Syst. Biol.* **2011**, *7*, 539.

(64) Stamm, M.; Staritzbichler, R.; Khafizov, K.; Forrest, L. R. AlignMe—a membrane protein sequence alignment web server. *Nucleic Acids Res.* **2014**, *42*, W246–W251.

(65) Sali, A.; Blundell, T. L. Comparative protein modelling by satisfaction of spatial restraints. *J. Mol. Biol.* **1993**, *234*, 779–815.

(66) Webb, B.; Sali, A. Protein structure modeling with MODELLER. *Methods Mol. Biol.* **2014**, *1137*, 1–15.

(67) Ramachandran, G. N.; Ramakrishnan, C.; Sasisekharan, V. Stereochemistry of polypeptide chain configurations. *J. Mol. Biol.* **1963**, *7*, 95–99.

(68) Wiederstein, M.; Sippl, M. J. ProSA-web: interactive web service for the recognition of errors in three-dimensional structures of proteins. *Nucleic Acids Res.* **2007**, *35*, W407–W410.

(69) *Molecular Operating Environment (MOE)*, 2014.09, Chemical Computing Group Inc., 1010 Sherbooke St. West, Suite #910, Montreal, QC, Canada, H3A 2R7, 2016.

(70) Halgren, T. A.; Murphy, R. B.; Friesner, R. A.; Beard, H. S.; Frye, L. L.; Pollard, W. T.; Banks, J. L. Glide: A new approach for rapid, accurate docking and scoring. 2.

Enrichment factors in database screening. *J. Med. Chem.* **2004**, *47*, 1750–1759.

(71)　　Friesner, R. A.; Banks, J. L.; Murphy, R. B.; Halgren, T. A.; Klicic, J. J.; Mainz, D. T.; Repasky, M. P.; Knoll, E. H.; Shaw, D. E.; Shelley, M.; Perry, J. K.; Francis, P.; Shenkin, P. S. Glide: A new approach for rapid, accurate docking and scoring. 1. Method and assessment of docking accuracy. *J. Med. Chem.* **2004**, *47*, 1739–1749

(72)　　Sherman, W.; Day, T.; Jacobson, M. P.; Friesner, R. A.; Farid, R. Novel procedure for modeling ligand/receptor induced fit effects. *J. Med. Chem.* **2006**, *49*, 534–553.

Table of Contents Graphic

Compound **61**

209x54mm (96 x 96 DPI)